

Ensemble Kalman filtering with residual nudging

By Xiaodong Luo^{*a} and Ibrahim Hoteit^b,

^a*International Research Institute of Stavanger, 5008 Bergen, Norway*

^b*King Abdullah University of Science and Technology, Thuwal, 23955-6900, Saudi Arabia*

6 November 2018

ABSTRACT

Covariance inflation and localization are two important techniques that are used to improve the performance of the ensemble Kalman filter (EnKF) by (in effect) adjusting the sample covariances of the estimates in the state space. In this work an additional auxiliary technique, called residual nudging, is proposed to monitor and, if necessary, adjust the residual norms of state estimates in the observation space. In an EnKF with residual nudging, if the residual norm of an analysis is larger than a pre-specified value, then the analysis is replaced by a new one whose residual norm is no larger than a pre-specified value. Otherwise the analysis is considered as a reasonable estimate and no change is made. A rule for choosing the pre-specified value is suggested. Based on this rule, the corresponding new state estimates are explicitly derived in case of linear observations. Numerical experiments in the 40-dimensional Lorenz 96 model show that introducing residual nudging to an EnKF may improve its accuracy and/or enhance its stability against filter divergence, especially in the small ensemble scenario.

1 Introduction

The ensemble Kalman filter (EnKF) (Anderson, 2001; Bishop et al., 2001; Burgers et al., 1998; Evensen, 1994; Hoteit et al., 2002; Houtekamer and Mitchell, 1998; Pham, 2001; Whitaker and Hamill, 2002) is an efficient algorithm for data assimilation in high dimensional systems. Because of its runtime efficiency and simplicity in implementation, it is receiving ever-increasing attentions from researchers in various fields. In many applications of the EnKF, due to limited computational resources, one is only able to run an EnKF with an ensemble size much smaller than the dimension of the state space. In such circumstances, problems often arise, noticeably on the quality of the sample covariances, including, for instance, rank-deficiency, underestimation of the covariance matrices (Sacher and Bartello, 2008; Whitaker and Hamill, 2002), and spuriously large cross-covariances between independent (or uncorrelated) state variables (Hamill et al., 2001). To mitigate these problems, it is customary to introduce two auxiliary techniques, namely covariance inflation (Anderson and Anderson, 1999) and localization (Hamill et al., 2001), to the EnKF. On the one hand, covariance inflation increases the estimated sample covariances in order to compensate for the effect of underestimation, which in fact increases the robustness of the EnKF in the sense of Luo and Hoteit (2011). On the other hand, covariance localization introduces a “distance”-dependent tapering function to the elements of the sample covariances, and smooths out the spuriously large values in them. In addition, covariance localization also increases the ranks of the sample covariances (Hamill et al., 2009).

Both covariance inflation and localization are techniques that in effect adjust the sample covariances in the state space. Since data assimilation is a practice of estimation that incorporates information from both the state and observation spaces, it would be natural for one to make use of the information in the observation space to improve the performance of an EnKF.

In this study we propose such an observation-space based auxiliary technique, called residual nudging, for the EnKF. Here a “residual” is a vector in the observation space, and is defined as the projection of an analysis mean onto the observation space subtracted from the corresponding observation. In residual nudging our objective is to make the vector norm of the residual (“residual norm” for short) no larger than a pre-specified value. This is motivated by the observation that, if the residual norm is too large, then the corresponding analysis mean is often a poor estimate. In such cases, it is better off to choose as the new estimate a state vector whose residual norm is smaller.

The method presented in this work is close to the idea of Van Leeuwen (2010), in which a nudging term is added to the particle filter so that the projections of the particles onto the observation space are drawn closer to the corresponding observation, and the particles themselves are associated with almost equal weights. By doing so, the modified particle filter can achieve remarkably good performance using only 20 particles in the chaotic 40-dimensional Lorenz-96 (L96) model (Lorenz and Emanuel, 1998), while traditional methods may need thousands of particles (Van Leeuwen, 2010). Other similar, residual-related, methods were also found in the literature, for examples, see Anderson (2007; 2009); Song et al. (2010). Anderson (2007; 2009) suggested adaptive covariance inflation schemes in the context of hierarchical ensemble filtering. There the inflation factor λ is

* Corresponding author.
e-mail: xiaodong.luo@iris.no

considered as a random variable (with a presumed initial prior distribution), and in effect adjusts the projection of the background (co)variances onto the observation space¹. With an incoming observation, the prior distribution is updated to the posterior one based on Bayes' rule, while the residual affects the shape of the posterior distribution of λ . On the other hand, Song et al. (2010) considered the idea of replacing an existing analysis ensemble member by a new one, in which the residual plays a role in generating the new ensemble member.

Our main purpose here is to use residual nudging as a safeguard strategy, with which the projections of state estimates onto the observation space, under suitable conditions, are guaranteed to be within a pre-specified distance to the corresponding observations. We will discuss how to choose the pre-specified distance, and construct the (possibly) new state estimates accordingly in case of linear observations. In this work, the ensemble adjustment Kalman filter (EAKF) (Anderson, 2001) is adopted for the purpose of demonstration, while the extension to other filters can be done in a similar way. Through numerical experiments in the L96 model, we show that, the EAKF equipped with residual nudging (EAKF-RN) is more robust than the normal EAKF. In addition, the accuracy of the EAKF-RN is comparable to, and sometimes (much) better than, that of the normal EAKF.

This work is organized as follows. Section 2 reviews the filtering step of the EAKF, introduces the concept of residual nudging, and discusses how it can be implemented in the EAKF. Section 3 investigates the effect of residual nudging on the performance of the Kalman filter (KF) in a linear/Gaussian system, which aims to provide some insights of how residual nudging may affect the behaviour of an already optimal filter. Section 4 extends the investigation to the Lorenz 96 model, in which we examine the performance of the EAKF-RN in various scenarios, and compare it with the normal EAKF. Section 5 discusses possible extensions of the current study and concludes the work.

2 Ensemble Kalman filtering with residual nudging

Suppose that at the k th assimilation cycle, one has a background ensemble $\mathbf{X}_k^b = \{\mathbf{x}_{k,i}^b\}_{i=1}^n$ with n members. The incoming observation \mathbf{y}_k^o is obtained from the following observation system

$$\mathbf{y}_k = \mathbf{H}_k \mathbf{x}_k + \mathbf{v}_k, \quad (1)$$

where \mathbf{H}_k is a matrix, and \mathbf{v}_k is the observation noise, with zero mean and covariance \mathbf{R}_k . For convenience of discussion, we assume that the dimensions of \mathbf{x}_k and \mathbf{y}_k are m_x and m_y , respectively, $m_y \leq m_x$, and \mathbf{H}_k has full row rank.

¹ In contrast, in residual nudging we are interested in adjusting the projection of the background mean. Comparison and/or combination of these two strategies will be deferred to future investigations.

2.1 The filtering step of the ensemble adjustment Kalman filter with covariance inflation and localization

We first summarize the filtering step of the EAKF with both covariance inflation and localization. For simplicity, here we only consider the scenario with constant covariance inflation and localization, and refer readers to, for example, Anderson (2007; 2009), for the details of adaptive configuration of the EAKF. In the context of EAKF, it is assumed that the covariance \mathbf{R}_k of the observation noise is a diagonal matrix, such that one can assimilate the incoming observation in a serial way. Following Anderson (2007; 2009), we use a single scalar observation to demonstrate the assimilation algorithm in the EAKF. To this end, in this sub-section (only) we temporarily assume that the observation vector $\mathbf{y}_k \equiv y_k$ is a scalar random variable, with zero mean and variance R_k . The notation of the incoming observation thus becomes y_k^o , with the dimension $m_y = 1$. The algorithm description below mainly follows Anderson (2007).

Suppose that the i -th ensemble member $\mathbf{x}_{k,i}^b$ of \mathbf{X}_k^b consists of m_x elements $(\mathbf{x}_{k,i}^b)_j$ ($j = 1, \dots, m_x$) such that $\mathbf{x}_{k,i}^b = [(\mathbf{x}_{k,i}^b)_1, \dots, (\mathbf{x}_{k,i}^b)_{m_x}]^T$. Then the sample mean $\hat{\mathbf{x}}_k^b$ of \mathbf{X}_k^b is $\hat{\mathbf{x}}_k^b = \sum_{i=1}^n \mathbf{x}_{k,i}^b / n$. To introduce covariance inflation to the filter, suppose that $\Delta \mathbf{X}_k^b \equiv \{\Delta \mathbf{x}_{k,i}^b : \Delta \mathbf{x}_{k,i}^b = \mathbf{x}_{k,i}^b - \hat{\mathbf{x}}_k^b\}_{i=1}^n$ is the ensemble of deviations with respect to \mathbf{X}_k^b , and $\lambda \geq 1$ the inflation factor, then the inflated background ensemble is $\mathbf{X}_k^{inf} \equiv \{\mathbf{x}_{k,i}^{inf} : \mathbf{x}_{k,i}^{inf} = \hat{\mathbf{x}}_k^b + \sqrt{\lambda} \Delta \mathbf{x}_{k,i}^b\}_{i=1}^n$ (Anderson, 2007; 2009). With covariance inflation, \mathbf{X}_k^{inf} and \mathbf{X}_k^b have the same mean, but the sample covariance of \mathbf{X}_k^{inf} is λ times that of \mathbf{X}_k^b . In what follows, we do not particularly distinguish background ensembles with and without covariance inflation through different notations. Instead, we always denote the background ensemble by \mathbf{X}_k^b , no matter whether it is inflated or not. One can tell whether a background ensemble is inflated by checking the value of λ , e.g., $\lambda = 1$ means no inflation, and $\lambda > 1$ with covariance inflation.

On the other hand, suppose that the projection of \mathbf{X}_k^b onto the observation space is $\mathbf{Y}_k^b = \{y_{k,i}^b : y_{k,i}^b = \mathbf{H}_k \mathbf{x}_{k,i}^b\}_{i=1}^n$, then one can compute the sample mean \hat{y}_k^b and sample variance $\hat{p}_{yy,k}^b$ as

$$\begin{aligned} \hat{y}_k^b &= \frac{1}{n} \sum_{i=1}^n y_{k,i}^b, \\ \hat{p}_{yy,k}^b &= \frac{1}{n-1} \sum_{i=1}^n (y_{k,i}^b - \hat{y}_k^b)^2. \end{aligned} \quad (2)$$

With the incoming observation y_k^o , one updates \hat{y}_k^b and $\hat{p}_{yy,k}^b$ to their analysis counterparts, \hat{y}_k^a and $\hat{p}_{yy,k}^a$, respectively, through the following formulae (Anderson, 2007, Eq. (3.2 - 3.3)).

$$\begin{aligned} \hat{p}_{yy,k}^a &= [(\hat{p}_{yy,k}^b)^{-1} + R_k^{-1}]^{-1}, \\ \hat{y}_k^a &= \hat{p}_{yy,k}^a [(\hat{p}_{yy,k}^b)^{-1} \hat{y}_k^b + R_k^{-1} y_k^o]. \end{aligned} \quad (3)$$

Accordingly, one can update the projection \mathbf{Y}_k^b to its analysis counterpart $\mathbf{Y}_k^a \equiv \{y_{k,i}^a : y_{k,i}^a = y_{k,i}^b + \delta y_{k,i}\}_{i=1}^n$, where the increments $\delta y_{k,i}$ with respect to $y_{k,i}^b$ are given by

$$\delta y_{k,i} = \sqrt{\frac{\hat{p}_{yy,k}^a}{\hat{p}_{yy,k}^b}} (y_{k,i}^b - \hat{y}_k^b) + \hat{y}_k^a - y_{k,i}^b. \quad (4)$$

One can verify that the sample mean and covariance of \mathbf{Y}_k^a are \hat{y}_k^a and $\hat{p}_{yy,k}^a$, respectively. Also note the difference between the concepts of deviations and increments. For distinction we have used Δ to denote deviations, and δ increments.

After the above quantities are calculated, one proceeds to update the background ensemble \mathbf{X}_k^b to the analysis one $\mathbf{X}_k^a \equiv \{\mathbf{x}_{k,i}^a : \mathbf{x}_{k,i}^a = \mathbf{x}_{k,i}^b + \delta\mathbf{x}_{k,i}\}_{i=1}^n$, where the increment $\delta\mathbf{x}_{k,i}$ with respect to the i -th background ensemble member $\mathbf{x}_{k,i}^b$ is an m_x dimensional vector, i.e., $\delta\mathbf{x}_{k,i} = [(\delta\mathbf{x}_{k,i})_1, \dots, (\delta\mathbf{x}_{k,i})_{m_x}]^T$, where the j -th element $(\delta\mathbf{x}_{k,i})_j$ of $\delta\mathbf{x}_{k,i}$ is given by

$$(\delta\mathbf{x}_{k,i})_j = (\hat{p}_{xy,k}^j / \hat{p}_{yy,k}^b) \delta y_{k,i}, j = 1, \dots, m_x, \quad (5)$$

with $\hat{p}_{xy,k}^j$ being the sample cross-variance between all the j -th elements of the ensemble members of \mathbf{X}_k^b , and the projection ensemble $\mathbf{Y}_k^b = \{y_{k,i}^b\}_{i=1}^n$, i.e.,

$$\hat{p}_{xy,k}^j = \frac{1}{n-1} \sum_{i=1}^n [(\mathbf{x}_{k,i}^b)_j - (\hat{\mathbf{x}}_k^b)_j][y_{k,i}^b - \hat{y}_k^b]. \quad (6)$$

With relatively small ensemble sizes, Eq. (6) often results in spuriously large sample cross-variances (Hamill et al., 2001). To tackle this problem, one may introduce covariance localization (Hamill et al., 2001) to the EAKF, in which the main idea is to multiply $\hat{p}_{xy,k}^j$ in Eq. (5) by a ‘‘distance’’-dependent tapering coefficient $\eta_{ij} \leq 1$ (Anderson, 2007; 2009). We will discuss how to compute η_{ij} in the experiments with respect to the L96 model.

After obtaining the analysis ensemble \mathbf{X}_k^a , one computes the analysis mean $\hat{\mathbf{x}}_k^a = \sum_{i=1}^n \mathbf{x}_{k,i}^a / n$ (analysis for short), and uses it as the posterior estimate of the system state. Propagating \mathbf{X}_k^a forward through the dynamical model, a background ensemble at the next assimilation time is obtained, and a new assimilation cycle starts, and so on.

2.2 Residual nudging

As will be shown later, the EAKF may suffer from filter divergence in certain circumstances, even when it is equipped with both covariance inflation and localization. To mitigate filter divergence, intuitively one may choose to adjust the estimate $\hat{\mathbf{x}}_k^a$ and move it closer toward the truth \mathbf{x}_k^{tr} . In practice, though, \mathbf{x}_k^{tr} is normally unknown, thus it is infeasible to apply this state-space based strategy. In what follows, we introduce a similar, but observation-space based strategy, in which the main idea is to monitor, and, if necessary, adjust the residual norm of the estimate. For this reason we refer to this strategy as residual nudging.

By definition, the residual with respect to the analysis mean $\hat{\mathbf{x}}_k^a$ is $\tilde{\mathbf{r}}_k^a \equiv \mathbf{H}_k \hat{\mathbf{x}}_k^a - \mathbf{y}_k^o$. We also define the 2-norm of a vector \mathbf{z} as

$$\|\mathbf{z}\|_2 \equiv \sqrt{\mathbf{z}^T \mathbf{z}}. \quad (7)$$

The objective in residual nudging is the following. We accept $\hat{\mathbf{x}}_k^a$ as a reasonable estimate if its residual norm $\|\tilde{\mathbf{r}}_k^a\|_2$ is no larger than a pre-specified value, say, $\beta \sqrt{\text{trace}(\mathbf{R}_k)}$, with $\beta > 0$ being called the noise level coefficient hereafter (the reason in choosing this pre-specified value will be explained soon). Otherwise, we consider $\hat{\mathbf{x}}_k^a$ a poor estimate, and thus find for it a replacement, say, $\tilde{\mathbf{x}}_k^a$, based on the estimate $\hat{\mathbf{x}}_k^a$ and the observation \mathbf{y}_k^o , so that the residual norm of $\tilde{\mathbf{x}}_k^a$ is

no larger than $\beta \sqrt{\text{trace}(\mathbf{R}_k)}$. To this end, we stress that the assumption $m_y \leq m_x$ may be necessary in certain cases (see the discussion later). In this work we focus on the cases with $m_y \leq m_x$, which is true for many geophysical problems.

The objective of residual nudging can be achieved as follows. First of all, we compute a scalar $c_k \in [0, 1]$, called the fraction coefficient hereafter (cf. Eq. (9a) later for the reason), according to the formula

$$c_k = \min(1, \beta \sqrt{\text{trace}(\mathbf{R}_k)} / \|\hat{\mathbf{r}}_k^a\|_2), \quad (8)$$

where the function $\min(a, b)$ finds the minimum between the scalars a and b . The rationale behind Eq. (8) is this: if $\|\hat{\mathbf{r}}_k^a\|_2 > \beta \sqrt{\text{trace}(\mathbf{R}_k)}$, then we need to multiply $\|\hat{\mathbf{r}}_k^a\|_2$ by a coefficient $c_k < 1$ to reduce $\|\hat{\mathbf{r}}_k^a\|_2$ to the pre-specified value. Otherwise, we do nothing and keep $\|\hat{\mathbf{r}}_k^a\|_2$ as it is, which is equivalent to multiplying $\|\hat{\mathbf{r}}_k^a\|_2$ by $c_k = 1$.

Next, we construct a new estimate $\tilde{\mathbf{x}}_k^a$ by letting

$$\tilde{\mathbf{x}}_k^a = c_k \hat{\mathbf{x}}_k^a + (1 - c_k) \mathbf{x}_k^o, \quad (9a)$$

$$\mathbf{x}_k^o = \mathbf{H}_k^T (\mathbf{H}_k \mathbf{H}_k^T)^{-1} \mathbf{y}_k^o. \quad (9b)$$

The term $\mathbf{H}_k^T (\mathbf{H}_k \mathbf{H}_k^T)^{-1}$ in Eq. (9b) is the Moore-Penrose generalized inverse of \mathbf{H}_k , such that \mathbf{x}_k^o in Eq. (9b) provides a least-square solution for the equation $\mathbf{H}_k \mathbf{x} = \mathbf{y}_k^o$ (Engl et al., 2000, ch. 2). We refer to \mathbf{x}_k^o as the observation inversion hereafter. With Eq. (9), the new residual $\tilde{\mathbf{r}}_k^a = \mathbf{H}_k \tilde{\mathbf{x}}_k^a - \mathbf{y}_k^o = c_k \hat{\mathbf{r}}_k^a$, so that $\|\tilde{\mathbf{r}}_k^a\|_2 = c_k \|\hat{\mathbf{r}}_k^a\|_2 \leq \beta \sqrt{\text{trace}(\mathbf{R}_k)}$ according to Eq. (8).

In residual nudging we only attempt to adjust the analysis mean $\hat{\mathbf{x}}_k^a$ of the EAKF, but not its covariance. To this end, let the analysis ensemble be $\mathbf{X}_k^a = \{\mathbf{x}_{k,i}^a : \mathbf{x}_{k,i}^a = \hat{\mathbf{x}}_k^a + \Delta\mathbf{x}_{k,i}^a\}_{i=1}^n$, where the deviations $\Delta\mathbf{x}_{k,i}^a = \mathbf{x}_{k,i}^a - \hat{\mathbf{x}}_k^a$. We then replace the original analysis mean $\hat{\mathbf{x}}_k^a$ by $\tilde{\mathbf{x}}_k^a$, and change the analysis ensemble to $\tilde{\mathbf{X}}_k^a = \{\tilde{\mathbf{x}}_{k,i}^a : \tilde{\mathbf{x}}_{k,i}^a = \tilde{\mathbf{x}}_k^a + \Delta\mathbf{x}_{k,i}^a\}_{i=1}^n$. Therefore, in comparison with the normal EAKF, the EAKF with residual nudging (EAKF-RN for short) just has additional steps in Eqs. (8) and (9), while all the other procedures remain the same. In doing so, residual nudging is compatible with both covariance inflation and localization.

2.3 Discussion

Choosing the pre-specified value in the form of $\beta \sqrt{\text{trace}(\mathbf{R}_k)}$ is motivated by the following consideration. Let \mathbf{x}_k^{tr} be the truth such that $\mathbf{y}_k^o = \mathbf{H}_k \mathbf{x}_k^{tr} + \mathbf{v}_k$. Then $\tilde{\mathbf{r}}_k^a = \mathbf{H}_k \tilde{\mathbf{x}}_k^a - \mathbf{y}_k^o = \mathbf{H}_k (\tilde{\mathbf{x}}_k^a - \mathbf{x}_k^{tr}) - \mathbf{v}_k$, and by the triangle inequality,

$$\|\tilde{\mathbf{r}}_k^a\|_2 \leq \|\mathbf{H}_k (\tilde{\mathbf{x}}_k^a - \mathbf{x}_k^{tr})\|_2 + \|\mathbf{v}_k\|_2. \quad (10)$$

For a reasonably good estimate $\tilde{\mathbf{x}}_k^a$, we expect that the magnitude of $\mathbf{H}_k \tilde{\mathbf{x}}_k^a - \mathbf{H}_k \mathbf{x}_k^{tr}$ should not substantially exceed the observation noise level. On the other hand, we have $(\mathbb{E}\|\mathbf{v}_k\|_2)^2 \leq \mathbb{E}\|\mathbf{v}_k\|_2^2 = \text{trace}(\mathbb{E}(\mathbf{v}_k \mathbf{v}_k^T)) = \text{trace}(\mathbf{R}_k)$, thus the expectation $\mathbb{E}\|\mathbf{v}_k\|_2$ of the norm of the observation noise is (at most) in the order of $\sqrt{\text{trace}(\mathbf{R}_k)}$. One may thus use $\sqrt{\text{trace}(\mathbf{R}_k)}$ to characterize the noise level. By requiring that a reasonably good estimate have $\|\mathbf{H}_k (\tilde{\mathbf{x}}_k^a - \mathbf{x}_k^{tr})\|_2$ in the order of $\sqrt{\text{trace}(\mathbf{R}_k)}$ (or less), one comes to the choice in the form of $\beta \sqrt{\text{trace}(\mathbf{R}_k)}$. The criterion in choosing the above threshold is very similar to that in certain quality control algorithms (called check of plausibility, see, for example Gandin, 1988, for a survey), in which one is assumed to have

prior knowledge about, say, the mean \bar{y}_s and variance σ_s of a scalar observation y_s . In quality control, y_s is often assumed to be a Gaussian random variable, so that for a measured observation y_s^o , if the ratio $|y_s^o - \bar{y}_s|/\sigma_s$ is too large, then y_s^o is discarded, or at least suspected (Gandin, 1988). The main differences between residual nudging and quality control are the following. While quality control checks the plausibility of an incoming observation, residual nudging checks the plausibility of a state estimate, and suggests a replacement if the original state estimate does not pass the test. Moreover, as long as the 2-norm is used, the expectation $\mathbb{E}\|\mathbf{v}_k\|_2^2$ is always $\text{trace}(\mathbf{R}_k)$, independent of the distribution of \mathbf{v}_k . This independence, on the one hand, implies that the inequality in (10), hence the threshold $\beta\sqrt{\text{trace}(\mathbf{R}_k)}$, holds without requiring the knowledge of the distribution of $\mathbf{H}_k(\tilde{\mathbf{x}}_k^a - \mathbf{x}_k^{tr})$. On the other hand, the absence of the knowledge of the distribution means that less statistical information is gained in choosing the threshold $\beta\sqrt{\text{trace}(\mathbf{R}_k)}$. For instance, one may not be able to assign a statistical meaning to $\beta\sqrt{\text{trace}(\mathbf{R}_k)}$, nor obtain a confidence (or significance) level in accepting (or rejecting) a state estimate. Finally, it is also possible for one to adopt another distance metric, e.g., the 1- or ∞ -norm, for which the inequality in (10) still holds. In such circumstances, the expectation, $\mathbb{E}\|\mathbf{v}\|_1^2$ or $\mathbb{E}\|\mathbf{v}_k\|_\infty^2$, may not be equal to $\text{trace}(\mathbf{R}_k)$ any more, so that one may need to choose a threshold different from $\beta\sqrt{\text{trace}(\mathbf{R}_k)}$. Despite the stated differences, we expect that residual nudging can be used in conjunction with observation quality control, although this is not pursued in the current study.

Even though the noise level coefficient β in residual nudging is chosen to be time-invariant, the resulting fraction coefficient c_k in general changes with time according to Eq. (8). The coefficient β affects how the new analysis $\tilde{\mathbf{x}}_k^a$ combines the original one $\hat{\mathbf{x}}_k^a$ and the observation inversion \mathbf{x}_k^o . This can be seen from Eqs. (8) and (9a). Because $c_k \in [0, 1]$, the new analysis $\tilde{\mathbf{x}}_k^a$ in Eq. (9a) is a convex combination of $\hat{\mathbf{x}}_k^a$ and \mathbf{x}_k^o , i.e., an estimate somewhere in-between the original estimate $\hat{\mathbf{x}}_k^a$ and the observation inversion \mathbf{x}_k^o , depending on the value of c_k . If one chooses a large value for β , or, if for a fixed β the original residual norm $\hat{\mathbf{r}}_k^a$ is sufficiently small, then the fraction coefficient $c_k \rightarrow 1$ according to Eq. (8), thus $\tilde{\mathbf{x}}_k^a \rightarrow \hat{\mathbf{x}}_k^a$ according to Eq. (9a). Therefore $\tilde{\mathbf{x}}_k^a$ will be a good estimate if $\hat{\mathbf{x}}_k^a$ is so, but may not be able to achieve a good estimation accuracy when $\hat{\mathbf{x}}_k^a$ itself is poor. On the other hand, if one chooses a very small value for β , or, if for a fixed β the original residual norm $\hat{\mathbf{r}}_k^a \rightarrow +\infty$ (e.g., with filter divergence), then $c_k \rightarrow 0$ and $\tilde{\mathbf{x}}_k^a \rightarrow \mathbf{x}_k^o$. In this case, the estimate $\tilde{\mathbf{x}}_k^a$ is calculated mainly based on the information content of the observation \mathbf{y}_k^o , and may result in a relatively poor accuracy. This is largely because of (1) the presence of the observation noise \mathbf{v}_k in Eq. (1), and (2) the ignorance of the prior knowledge of the model dynamics. As a result, pushing the projection of state estimates very close to noisy observations may have some negative consequences. For instance, in geophysical applications, dynamical balances of the numerical models may not be honored so that the estimation errors may be relatively large. However, using \mathbf{x}_k^o as the estimate may be a relatively safe (although conservative) strategy against filter divergence. In the sense of the above discussion, the choice of β reflects the extent to which one wants to achieve the trade-off between a filter's poten-

tial accuracy and stability against divergence. This point is further demonstrated through some experiments later.

Some numerical issues related to the computation of the observation inversion \mathbf{x}_k^o are discussed in order. One is the existence and uniqueness of the observation inversion. Under the assumptions that $m_y \leq m_x$ and that \mathbf{H}_k is of full row rank, the observation inversion, as a solution of the equation $\mathbf{H}_k \mathbf{x} = \mathbf{y}_k^o$, does exist (Meyer, 2001, ch. 4). Finding a concrete solution, however, is in general an under-determined problem, hence the solution is not unique unless $m_y = m_x$. This point can be seen as follows. When $m_y < m_x$, the null space \mathbb{S}^N of \mathbf{H}_k contains non-zero elements, i.e., there exist elements $\mathbf{x}_n \in \mathbb{S}^N$, $\mathbf{x}_n \neq \mathbf{0}$, such that $\mathbf{H}_k \mathbf{x}_n = \mathbf{0}$ (Meyer, 2001, ch. 4). As a result, given an observation inversion \mathbf{x}_k^o , $\mathbf{x}_k^o + \mathbf{x}_n$ is also a solution of the equation $\mathbf{H}_k \mathbf{x} = \mathbf{y}_k^o$ for any $\mathbf{x}_n \in \mathbb{S}^N$. Therefore, which solution one should take is an open problem in practice. In the context of state estimation, it is desirable to choose a solution that is close to the truth \mathbf{x}_k^{tr} , which, unfortunately, is infeasible without the knowledge of \mathbf{x}_k^{tr} . As a trade-off, one may choose as a solution some estimate that possesses certain properties. The Moore-Penrose generalized inverse \mathbf{x}_k^o given in Eq. (9b) is such a choice, which is the unique, and “best-approximate”, solution in the sense that it has the minimum 2-norm among all least-squares solutions (Engl et al., 2000, Theorem 2.5).

It is also worth mentioning what may happen if our assumptions, that $m_y \leq m_x$ and that \mathbf{H}_k is of full row rank, are not valid. In the former case, with $m_y > m_x$, the equation $\mathbf{H}_k \mathbf{x} = \mathbf{y}_k^o$ is over-determined, meaning that there may be no solution that solves the equation exactly. One may still obtain an approximate solution by recasting the problem of solving the linear equation as a linear least-squares problem, which yields the unique, least-squares solution in the form of $\mathbf{x}_k^o = (\mathbf{H}_k^T \mathbf{H}_k)^{-1} \mathbf{H}_k^T \mathbf{y}_k^o$, similar to (but different from) Eq. (9b). Because $\mathbf{H}_k \mathbf{x}_k^o - \mathbf{y}_k^o$ may not be $\mathbf{0}$ in general, one may thus not be able to find a new estimate $\tilde{\mathbf{x}}_k^a$ with a sufficiently small (e.g., zero) residual. Therefore, the inequality $\|\tilde{\mathbf{r}}_k^a\|_2 \leq \beta\sqrt{\text{trace}(\mathbf{R}_k)}$ may not hold for some sufficiently small β . This restriction is consistent with the nature of over-determined problems (that is, no exact solution). It does not necessarily mean that residual nudging cannot be applied to an over-determined problem, but instead implies that the noise level coefficient β should entail a lower bound that may be larger than 0.

In the latter case, without loss of generality, suppose that $m_y \leq m_x$ and \mathbf{H}_k is not of full row rank, then the matrix product $\mathbf{H}_k \mathbf{H}_k^T$ is singular, so that it may be numerically unstable to compute its inverse. In such circumstances, one needs to employ a certain regularization technique to obtain an approximate, but stable, solution. For instance, one may adopt the Tikhonov regularization (Engl et al., 2000, ch. 4) so that the solution in Eq. (9b) becomes $\mathbf{x}_k^o = \mathbf{H}_k^T (\mathbf{H}_k \mathbf{H}_k^T + \alpha \mathbf{I})^{-1} \mathbf{y}_k^o$, where α is the regularization parameter chosen according to a certain criterion. The observation inversion in Eq. (9b) can be treated as a special case of the Tikhonov regularization solution with $\alpha = 0$, while the concept of residual nudging is also applicable to the general cases with $\alpha \neq 0$ following our deduction in § 2.2². In this sense, the state estimate of the EAKF-RN

² In general cases with $\alpha \neq 0$, it can be shown that a sufficient

can be considered as a hybrid of the original EAKF estimate and the (regularized) least-squares solution of the equation $\mathbf{H}_k \mathbf{x} = \mathbf{y}_k^o$. This point of view opens up many other possibilities, given the various types of regularization techniques in the literature (see, for example, Engl et al. 2000).

The computation of the matrix product $\mathbf{H}_k^T (\mathbf{H}_k \mathbf{H}_k^T)^{-1}$ is a non-trivial issue in large-scale problems, and is worthy of further discussion³. In general cases where the observation operator \mathbf{H}_k is time varying, the computational cost is comparable to that in evaluating the Kalman gain. In terms of numerical computations, one possible choice is to apply QR factorization (Meyer, 2001, ch. 5) to \mathbf{H}_k^T such that \mathbf{H}_k^T is factorized as the product of an orthogonal, $m_x \times m_x$ matrix \mathbf{Q} and an upper-triangular, $m_x \times m_y$ matrix \mathbf{U} , where for notational convenience we drop the time index k in these matrices. Note that $\mathbf{Q}\mathbf{Q}^T = \mathbf{Q}^T\mathbf{Q} = \mathbf{I}_{m_x}$, and $\mathbf{U} = [\mathbf{U}_{m_y}^T, \mathbf{0}_{(m_x-m_y)m_y}^T]^T$, with \mathbf{I}_{m_x} being the m_x -dimensional identity matrix, $\mathbf{0}_{(m_x-m_y)m_y}$ the $(m_x - m_y) \times m_y$ zero matrix, and \mathbf{U}_{m_y} a non-singular, upper-triangular, $m_y \times m_y$ matrix in which all elements below the main diagonal are zero. With some algebra, it can be shown that the product $\mathbf{H}_k^T (\mathbf{H}_k \mathbf{H}_k^T)^{-1} = \mathbf{Q} [\mathbf{U}_{m_y}^{-1}, \mathbf{0}_{(m_x-m_y)m_y}]^T = \mathbf{Q}_{m_x m_y} (\mathbf{U}_{m_y}^{-1})^T$, where $\mathbf{Q}_{m_x m_y}$ is a matrix that is comprised of the first m_y columns of \mathbf{Q} , and the inverse $\mathbf{U}_{m_y}^{-1}$ of the upper-triangular matrix \mathbf{U}_{m_y} can be computed element-by-element in a recursive way (called back substitution, Meyer 2001, ch. 5). In certain circumstances, further reduction of computational cost and/or storage can be achieved, for instance, when \mathbf{H}_k is sparse (Meyer, 2001, ch. 5); or when \mathbf{H}_k is time invariant, e.g., in a static observation network. In the latter case, one only needs to evaluate the product $\mathbf{H}_k^T (\mathbf{H}_k \mathbf{H}_k^T)^{-1}$ once and for all.

3 Numerical results in a linear scalar system

Here we use a scalar, first order autoregressive (AR1) model driven by Gaussian white noise, to investigate the performance of the Kalman filter (KF, Kalman, 1960), and that of the KF with residual nudging (KF-RN), in which residual nudging is introduced to the posterior estimate of the KF in the same way as in the EAKF. The motivation in conducting this experiment is the following. With linear and Gaussian observations, the KF provides the optimal estimate in the sense of, for instance, minimum variance (Jazwinski, 1970). Therefore, we use the KF estimate as the reference to examine the behaviour of the KF-RN under different settings, which reveals how residual nudging may affect the performance of the KF.

The scalar AR1 model is given by

$$x_{k+1} = 0.9 x_k + u_k, \quad (11)$$

where u_k represents the dynamical noise and follows the

condition to achieve residual nudging is, for example, $c_k (\|\hat{\mathbf{x}}_k^a\|_2 - \|\mathbf{y}_k^o\|_2) \leq \beta \sqrt{\text{trace}(\hat{\mathbf{R}}_k)} - \|\mathbf{y}_k^o\|_2$, with the (possibly) new estimate $\hat{\mathbf{x}}_k^a$ again given by Eq. (9a).

³ For the experiments to be presented later, since the dimensions of the dynamical models are relatively low, we choose to directly compute the matrix product $\mathbf{H}_k^T (\mathbf{H}_k \mathbf{H}_k^T)^{-1}$. The matrix inversion $(\mathbf{H}_k \mathbf{H}_k^T)^{-1}$ is done through the MATLAB (R2011b) built-in function INV.

Gaussian distribution with zero mean and variance 1, and is thus denoted by $u_k \sim N(u_k : 0, 1)$. The observation model is described by

$$y_k = x_k + v_k, \quad (12)$$

where $v_k \sim N(v_k : 0, 1)$ is the observation noise, and is uncorrelated with u_k .

In the experiment, we integrate the AR1 model forward for 10,000 steps (integration steps hereafter), with the initial value randomly drawn from the Gaussian distribution $N(0, 1)$, and the associated initial prior variance being 1. The true states (truth) $\{x_k\}_{i=1}^{10000}$ are obtained by drawing samples of dynamical noise from the distribution $N(0, 1)$, and adding them to x_k to obtain x_{k+1} at the next integration step, and so on. The synthetic observations y_k^o are obtained by adding to model states x_k samples of observation noise from the distribution $N(0, 1)$. For convenience of comparison, we generate and store synthetic observations at every integration step. However, we choose to assimilate them for every S_a integration steps, with $S_a \in \{1, 2, 4, 8\}$, in order to investigate the impact of S_a on filter performance. In doing so, data assimilation with different S_a , or other experiment settings (e.g., the noise level coefficient β in the KF-RN), will have identical observations at the same integration steps. For convenience, hereafter we may sometimes use the concept ‘‘assimilation step’’, with one assimilation step equal to S_a integration steps. In addition, we may also call S_a the assimilation step when it causes no confusion.

In the KF-RN, we also choose to vary the noise level coefficient β , with $\beta \in \{0.01, 0.05, 0.1, 0.5, 1, 2, 3, 4, 6, 8, 10\}$, in order to investigate its effect on filter performance. To reduce statistical fluctuations, we repeat the experiment 20 times, each time with randomly drawn initial value, samples of dynamical and observation noise (so that the truth and the corresponding observations are produced at random). Except for the introduction of residual nudging, the KF-RN have the same configurations and experiment settings as the KF.

We use the average root mean squared error (average RMSE) to measure the accuracy of a filter estimate. For an m_x -dimensional system, the RMSE e_k of an estimate $\hat{\mathbf{x}}_k = [\hat{x}_{k,1}, \dots, \hat{x}_{k,m_x}]^T$ with respect to the true state vector $\mathbf{x}_k^{tr} = [x_{k,1}^{tr}, \dots, x_{k,m_x}^{tr}]^T$ at time instant k is defined as

$$e_k = \|\hat{\mathbf{x}}_k - \mathbf{x}_k^{tr}\|_2 / \sqrt{m_x}. \quad (13)$$

The average RMSE \hat{e}_k at time instant k over M repetitions of the same experiment is thus defined as $\hat{e}_k = \sum_{j=1}^M e_k^j / M$ ($M = 20$ in our setting), where e_k^j denotes the RMSE at time instant k in the j th repetition of the experiment. We also define the time mean RMSE \hat{e} as the average of \hat{e}_k over the assimilation time window with N integration steps, i.e., $\hat{e} = \sum_{i=1}^N \hat{e}_k / N$ ($N = 10000$ here).

We also use the spread to measure the estimated uncertainty associated with an estimation. To this end, let $\hat{\mathbf{P}}_k$ be the estimated covariance matrix with respect to the estimate $\hat{\mathbf{x}}_k$. Then the spread s_k at time instant k is defined as

$$s_k = \sqrt{\text{trace}(\hat{\mathbf{P}}_k) / m_x}. \quad (14)$$

The average spread \hat{s}_k and the time mean (average) spread

\hat{s} are defined in a way similar to their counterparts with respect to the RMSE.

Table 1 reports the time mean RMSEs and spreads of the KF at different assimilation steps S_a . The time mean RMSE of the KF grows as S_a increases, indicating that the performance of the KF deteriorates as the assimilation frequency decreases. The time mean spread of the KF exhibits a similar tendency as S_a increases. However, the time mean spread tends to be larger than the time mean RMSE, indicating that the corresponding variance is over-estimated.

Fig. 1 shows the time mean RMSEs of the KF-RN (dash-dot lines marked by diamonds), as functions of the noise level coefficient β , at different assimilation steps S_a . Given the different orders of magnitudes of β , we adopt the logarithmic scale for the x-axes. For comparison, we also plot the time mean RMSEs of the KF (solid lines) at each S_a . Since the time mean RMSEs of the KF are independent of the choice of β , they are horizontal lines in the plots. However, the choice of β does influence the performance of the KF-RN. As shown in all of the plots of Fig. 1, if one adopts a small β , say $\beta = 0.01$, for the KF-RN, then the resulting time mean RMSE is higher than that of the KF. This is because such a choice may force the KF-RN to rely excessively on the observations when updating the prior estimates, such that the information contents in the prior estimates are largely ignored. As β grows, the time mean RMSE of the KF-RN decreases, and eventually converges to that of the KF when β is sufficiently large, say $\beta \geq 3$. These results are consistent with our expectation of the behaviour of a filter equipped with residual nudging, as has been discussed in § 2.3.

It is also of interest to gain some insights of the behaviour of the fraction coefficients c_k in the KF-RN with different β . To this end, Fig. 2 plots two sample time series of c_k in the KF-RN with $\beta = 0.1$ (upper left panel), and $\beta = 1$ (lower left panel), respectively, together with their corresponding histograms (right panels). For convenience of visualization, the assimilation time window is shortened to 1000 steps (with the observations assimilated for every 4 steps). At $\beta = 0.1$, c_k tends to be relatively small, with the mean value being 0.4213 and the median 0.3027. Among the 250 c_k values, 210 of them are less than 1, meaning that residual nudging is effective at those steps. A histogram of c_k is also shown on the upper right panel. There it indicates that c_k distributes like a U-shape, with relatively large proportions of c_k taking values that are less than 0.2, or equal to 1. On the other hand, at $\beta = 1$, c_k tends to remain close to 1, with the mean being 0.9892 and the median 1, and only 16 out of 250 c_k values are less than 1. These are also manifested in the histogram on the lower right panel, where one can see that c_k largely concentrate on 1.

In Table 1 we report the minimum time mean RMSEs that the KF-RN can achieve by varying the value of β at different S_a , together with the values of the β at which the minima are obtained for specific S_a . When $S_a = 1, 2$, the minimum time mean RMSEs of the KF-RN, both achieved at $\beta = 2$, are (very) slightly lower than the time mean RMSEs of the KF; and the time mean RMSEs of the KF-RN become the same as those of the KF when $\beta \geq 3$. On the other hand, when $S_a = 4, 8$, the minimum time mean RMSEs of the KF-RN are identical to the time mean RMSEs of the KF, and are obtained when $\beta \geq 2$. The reason that the

KF-RN can have lower time mean RMSEs than the “optimal” KF at $S_a = 1, 2$ might be the following. The classic filtering theory states that the KF is optimal under the minimum variance (MV) criterion (Jazwinski, 1970), that is, taking the mean of the posterior conditional pdf as the state estimate, the KF has the lowest possible expectation of squared estimation error. Note that here the expectation is taken over all possible values of the truth (i.e., by treating the truth as a random variable). Therefore, in principle one has to repeat the same experiment for a sufficiently large number of times (with randomly drawn truth) in order to verify the performance of the filters under the MV criterion. For computational convenience, though, we only repeat the experiment 20 times. Thus in our opinion the slight out-performance of the KF-RN might be largely attributed to statistical fluctuations.

In Table 1 we do not present the time mean spreads of the KF-RN because they are in fact identical to those of the KF. This is because in the KF, the forecast and update of the (estimated) covariance matrix of the system state are not influenced by the mean estimate of the system state (Jazwinski, 1970). Since residual nudging only changes the estimate of the system state (if necessary) and nothing else, it is expected that the KF and KF-RN share the same covariance matrix. This point, however, is not necessarily true in the context of ensemble filtering in a nonlinear system. For instance, if the dynamical model is nonlinear, then the background covariance at the next assimilation time is affected by the analysis mean at the current time, such that two analysis ensembles with different sample (analysis) means but identical sample (analysis) covariance may result in different sample (background) means and covariances at the next assimilation time.

The above results suggest that it may not be very meaningful to introduce residual nudging to a Bayesian filter that already performs well. In practice, though, due to the existence of various sources of uncertainties (Anderson, 2007; Luo and Hoteit, 2011), a Bayesian filter is often sub-optimal, and is even likely to suffer from divergence (Schlee et al., 1967). In such circumstances, instead of only looking into the accuracy of a filter, it may also be desirable to take the stability of the filter into account. Through the experiments below we show that equipping the EAKF with residual nudging can not only help improve its stability, but also achieve a filter accuracy that is comparable to, sometimes even (much) better than, that of the normal EAKF, especially in the small ensemble scenario.

4 Numerical results in the 40-dimensional L96 model

4.1 Experiment settings

Here we use the 40-dimensional Lorenz-96 (L96) model (Lorenz and Emanuel, 1998) as the testbed. The governing equations of the L96 model are given by

$$\frac{dx_i}{dt} = (x_{i+1} - x_{i-2})x_{i-1} - x_i + F, \quad i = 1, \dots, 40. \quad (15)$$

The quadratic terms simulate advection, the linear term represents internal dissipation, and F acts as the external forcing term (Lorenz, 1996). Throughout this work, we choose

618 $F = 8$ unless otherwise stated. For consistency, we define 672
 619 $x_{-1} = x_{39}$, $x_0 = x_{40}$, and $x_{41} = x_1$ in Eq. (15), and con- 673
 620 struct the state vector $\mathbf{x} \equiv [x_1, x_2, \dots, x_{40}]^T$.

621 We use the fourth-order Runge-Kutta method to inte- 674
 622 grate (and discretize) the system from time 0 to 75, with 675
 623 a constant integration step of 0.05. To avoid the transition 676
 624 effect, we discard the trajectory between 0 and 25, and use 677
 625 the rest for data assimilation. The synthetic observation \mathbf{y}_k 678
 626 is obtained by measuring (with observation noise) every d 679
 627 elements of the state vector $\mathbf{x}_k = [x_{k,1}, x_{k,2}, \dots, x_{k,40}]^T$ at 680
 628 time instant k , i.e.,

$$629 \quad \mathbf{y}_k = \mathbf{H}^d \mathbf{x}_k + \mathbf{v}_k, \quad (16)$$

630 where \mathbf{H}^d is a $(J+1) \times 40$ matrix such that $\mathbf{H}^d \mathbf{x}_k =$ 682
 631 $[x_{k,1}, x_{k,1+d}, \dots, x_{k,1+Jd}]^T$, with $J = \text{floor}(39/d)$ being the 683
 632 largest integer that is less than, or equal to, $39/d$, and \mathbf{v}_k 684
 633 is the observation noise following the Gaussian distribution 685
 634 $N(\mathbf{v}_k : \mathbf{0}, \mathbf{I}_{J+1})$, with \mathbf{I}_{J+1} being the $(J+1)$ -dimensional 686
 635 identity matrix. The elements $(\mathbf{H}^d)_{pq}$ of the matrix \mathbf{H}^d can 687
 636 be determined as follows.

$$637 \quad (\mathbf{H}^d)_{pq} = 1 \text{ if } q = (p-1)d + 1, \text{ otherwise } (\mathbf{H}^d)_{pq} = 0,$$

638 for $p = 1, \dots, (J+1)$, $q = 1, \dots, 40$. In all the experiments 692
 639 below, we generate and store the synthetic observations at 693
 640 every integration step, but assimilate the observations for 694
 641 every 4 integration steps unless otherwise stated. 695

642 The filters in the experiments are configured as fol- 696
 643 lows. To generate an initial background ensemble, we run 697
 644 the L96 model from 0 to 2500 (overall 50000 integra- 698
 645 tion steps), and compute the temporal mean and covari- 699
 646 ance of the trajectory⁴. We then assume that the ini- 700
 647 tial state vectors follow the Gaussian distribution with the 701
 648 same mean and covariance, and draw a specified number 702
 649 of samples to form the background ensemble. Covariance 703
 650 inflation (Anderson and Anderson, 1999) and localization 704
 651 (Hamill et al., 2001) are conducted in all the experiments. 705
 652 Concretely, covariance inflation, with the inflation factor λ , 706
 653 is introduced following the discussion in § 2.1. Covariance 707
 654 localization is conducted following Anderson (2007; 2009), 708
 655 which introduces an additional parameter l_c , called the 709
 656 length scale (or half-width following Anderson 2007; 2009) 710
 657 hereafter, to the EAKF. The distance d_{ij} between two state 711
 658 variables x_i and x_j are defined as $d_{ij} = \min(|i-j|/40, 1 -$ 712
 659 $|i-j|/40)$, and the corresponding tapering coefficient η_{ij} 713
 660 (cf. the text below Eq. (6)) is determined by the fifth-order 714
 661 polynomial function $\xi(d_{ij}, l_c)$ in Gaspari and Cohn (1999) 715
 662 with half-width l_c . For $d_{ij} < 2l_c$, one has $0 < \eta_{ij} \leq 1$, and 716
 663 $\eta_{ij} = 0$ otherwise. With both covariance inflation and local- 717
 664 ization, the performance of the normal EAKF is in general 718
 665 comparable to the established results with respect to the 719
 666 L96 model under similar experiment setting, see, for exam- 720
 667 ple, Fertig et al. (2007); Hunt et al. (2004). 721

668 To reduce statistical fluctuations, we repeat each exper- 722
 669 iment below for 20 times, each time with randomly drawn 723
 670 initial state vector, initial background ensembles and obser- 724
 671 vations. Except for the introduction of residual nudging, in 725

all experiments the normal EAKF and the EAKF-RN have 726
 identical configurations and experiment settings. 727

4.2 Experiment results

4.2.1 Results with different observation operators 728
 Here we 729
 consider four different observation operators \mathbf{H}^d , with $d =$ 730
 1, 2, 4, 8, respectively. For convenience, we refer to them as 731
 the full, 1/2, 1/4 and 1/8 observation scenarios, respectively. 732
 The concrete configurations of the normal EAKF and the 733
 EAKF-RN are the following. In both filters the ensemble size 734
 is fixed to be 20. The half-width l_c of covariance localization 735
 increases from 0.1 to 0.5, each time with an even increment 736
 of 0.1. For convenience we denote this setting by $l_c \in \{0.1 :$ 737
 0.1 : 0.5}. Similar notations will be frequently used later. 738
 The inflation factor $\lambda \in \{1 : 0.05 : 1.25\}$, and the noise level 739
 coefficient $\beta = 2$ in the EAKF-RN. 740

The upper panels of Fig. 3 shows the contour plots of 741
 the time mean RMSEs of the normal EAKF (left), and that 742
 of the EAKF-RN (right), in the full observation scenario, 743
 as functions of the inflation factor λ and the half-width l_c . 744
 Given a fixed λ , the time mean RMSEs of both the EAKF 745
 and EAKF-RN tend to increase as the half-width l_c in- 746
 creases. On the other hand, given a fixed l_c , when $l_c = 0.1$, 747
 the time mean RMSEs of both filters exhibit the U-turn be- 748
 haviour, i.e., the time mean RMSEs tend to decrease as λ 749
 grows, until it reaches a certain value (1.10 for both filters). 750
 After that, the time mean RMSEs will increase instead as λ 751
 grows further. However, when $l_c > 0.1$, the time mean RM- 752
 SEs of both filters tend to decrease as λ increases within the 753
 range of tested λ . The normal EAKF achieves its minimum 754
 time mean RMSE (0.5605) at the point ($l_c = 0.1, \lambda = 1.10$), 755
 and the EAKF-RN also hits its minimum time mean RMSE 756
 (0.5586) at the same place. In general, the EAKF and the 757
 EAKF-RN have similar performance at $l_c = 0.1$, but at other 758
 places the EAKF-RN may perform substantially better than 759
 the EAKF. For instance, at ($l_c = 0.4, \lambda = 1.05$) the time 760
 mean RMSE of the normal EAKF is about 3.3, while that of 761
 the EAKF-RN is about 1.6. Moreover, a filter divergence 762
 is spotted in the normal EAKF at ($l_c = 0.3, \lambda = 1.25$), so 763
 that the contour plot around this point is empty and indi- 764
 cates no RMSE value. Filter divergence, however, is not ob- 765
 served in the EAKF-RN at the same place. For clarity, here 766
 a ‘‘divergence’’ is identified as an event in which the RMSE 767
 of a filter becomes abnormally large. More specifically, the 768
 filter is considered divergent in the Lorenz 96 model, if its 769
 RMSE at any particular time instant is larger than 10^3 . As 770
 mentioned previously, we repeat each experiment 20 times in 771
 order to reduce statistical fluctuations. In accordance with 772
 this setting, a filter divergence is reported whenever there is 773
 at least one (but not necessarily all) divergence(s) out of 20 774
 repetitions. 775

In the 1/2 and 1/4 observation scenarios, there are 776
 many cases in which filter divergences are spotted. For this 777
 reason, we choose to directly report the assimilation results 778
 in Tables 2 and 3, respectively, rather than show their con- 779
 tour plots as in the full observation scenario. In the 1/2 ob- 780
 servation scenario, filter divergences of the normal EAKF, 781
 marked by ‘‘Div’’ in Table 2, are spotted in 24 out of 30 782
 different combinations of l_c and λ values (5 l_c values by 783
 6 λ values). In contrast, in the EAKF-RN no filter diver- 784
 gence is observed. On the other hand, when there is no fil- 785

⁴ Let $\{\mathbf{x}_k\}_{k=1}^N$ be a set of state vectors at different time instants 786
 which form a state trajectory from time instant 1 to N . Then the 787
 temporal mean and covariance of the trajectory are taken as the 788
 sample mean and covariance of the set $\{\mathbf{x}_k\}_{k=1}^N$, respectively. 789

ter divergence occurring in either filter, the performance of the EAKF and the EAKF-RN is very close to each other, with the time mean RMSEs of the EAKF-RN slightly lower than those of the EAKF, except at ($l_c = 0.1, \lambda = 1.15$) and ($l_c = 0.1, \lambda = 1.25$). The situation in the 1/4 observation is similar. As shown in Table 3, the EAKF diverges in 17 out of 30 tested cases, while there is no filter divergence spotted in the EAKF-RN. The performance of the EAKF and the EAKF-RN is close to each other when the EAKF does not diverge.

The lower panels of Fig. 3 shows the contour plots of the time mean RMSEs of the normal EAKF (left), and that of the EAKF-RN (right), in the 1/8 observation scenario. In this scenario, no filter divergence is spotted in the EAKF. Overall, the performance of the EAKF and the EAKF-RN is very close to each other, although the EAKF-RN has a slightly lower minimum time mean RMSE (2.9556 achieved at ($l_c = 0.1, \lambda = 1$)) than that of the EAKF (2.9619 obtained at the same place).

We then examine the impact of residual nudging on the time mean spreads of the filters in different observation scenarios. For the full and 1/8 observation scenarios, we plot the time mean spreads of the EAKF and the EAKF-RN in Fig. 4; while for the 1/2 and 1/4 observation scenarios, we report them in Tables 2 and 3, in the parentheses after the RMSE values. In all the reported cases in which the EAKF does not diverge, the time mean spreads of the EAKF-RN in general do not significantly deviate from those of the EAKF. In cases that the EAKF does diverge, the EAKF-RN may still maintain positive and finite time mean spreads. The closeness of the time mean spreads of the EAKF and EAKF-RN in the former cases, though, may depend on the experiment settings, e.g., the choice of the noise level coefficient β . However, from our experience, as long as β is reasonably large (say $\beta \geq 2$), the time mean spread of the EAKF-RN often approaches that of the EAKF. For brevity, hereafter we do not report the spread values any more.

Overall, in both the normal EAKF and the EAKF-RN, their time mean RMSEs tend to increase as the number of elements in an observation decreases. The performance of the EAKF-RN, in terms of time mean RMSE, is in general comparable to, and sometimes (substantially) better than, that of the EAKF. Moreover, the EAKF-RN tends to perform more stably than the EAKF.

4.2.2 Results with different noise level coefficients Next we examine the effect of the noise level coefficient β on the performance of the EAKF-RN. The experiment settings are as follows. We conduct the experiments in four observation scenarios as in the previous experiment. The ensemble size of the EAKF-RN is 20. We choose the noise level coefficient β from the sets $\{0\}$, $\{0.02 : 0.02 : 0.1\}$, $\{0.2 : 0.2 : 1\}$, and $\{2, 3, 4, 6, 8\}$. The reason to single out $\beta = 0$ will be given soon. Under the above setting, it is infeasible for us to adopt too many combinations of l_c and λ as in the previous experiment, either for presentation or computation. Therefore, we only choose two such combinations in the current experiment (similar choices will also be made in subsequent experiments, in which we can only afford to vary some of the parameter values, and have to freeze the rest). In the first combination we let $l_c = 0.1$ and $\lambda = 1.15$, and in the

second $l_c = 0.3$ and $\lambda = 1.05$. From the previous experiment results, the former choice represents a relatively good filter configuration for the normal EAKF, while the latter a less proper one. We thus use these two configurations to illustrate the effect of residual nudging when the normal EAKF has reasonable/(relatively) poor performance.

Fig. 5 depicts the time mean RMSEs of the EAKF-RN as functions of β in different observation scenarios, in which the relatively good filter configuration $l_c = 0.1$ and $\lambda = 1.15$ is adopted. Due to different orders of magnitudes of β , the x-axes are all plotted in the logarithmic scale. For this reason, it is inconvenient to show the results of $\beta = 0$ at $\log 0 (= -\infty)$. Instead, we plot the results at $\beta = 0.005$, and “artificially” label that point 0. The time mean RMSEs of the normal EAKF are independent of β , and are plotted as horizontal lines in the relevant sub-figures (if no filter divergence in the normal EAKF). In all observation scenarios, the time mean RMSEs of the EAKF-RN are relatively large at small β values (say $\beta = 0.02$). As β increases, the time mean RMSEs of the EAKF-RN tend to converge to those of the normal EAKF. During the processes of convergence, the minimum time mean RMSE of the EAKF-RN in the full observation scenario is lower than that of the normal EAKF, while the minimum time mean RMSEs of the EAKF-RN in other observation scenarios are either indistinguishable from (in the 1/2 and 1/4 observation scenarios), or slightly higher than (in the 1/8 observation scenario), those of the normal EAKF.

Fig. 6 shows the time mean RMSEs of the normal EAKF and the EAKF-RN, with experiment settings similar to those in Fig. 5, except that the covariance localization and inflation configuration becomes $l_c = 0.3$ and $\lambda = 1.05$, respectively, which, as will be shown below, makes the normal EAKF perform worse in comparison to the previous case in Fig. 5.

With $l_c = 0.3$ and $\lambda = 1.05$, the resulting EAKF-RN behaves similarly to that with the previous configuration $l_c = 0.1$ and $\lambda = 1.15$. For the current filter configuration, though, as β grows, the time mean RMSEs of the EAKF-RN exhibit clear troughs in all observation scenarios. On the other hand, compared to the previous results in Fig. 5, the performance of the normal EAKF deteriorates in all observation scenarios. Indeed, with the current filter configuration, the normal EAKF may perform (substantially) worse than the EAKF-RN under the same experiment settings, especially if a proper β value is chosen for the EAKF-RN. In particular, the normal EAKF diverges in the 1/2 (upper right) and 1/4 (lower left) observation scenarios, while no filter divergence is spotted in the EAKF-RN with $\beta \leq 3$, although the EAKF-RN does diverge in the 1/2 and 1/4 observation scenarios, given $\beta \geq 4$. This suggests that one may increase the stability of the EAKF-RN against filter divergence by decreasing the value of β , so that c_k is closer to 0 and the observation inversion becomes more influential in Eq. (9a), as we have discussed in §2.3.

It is also worth mentioning the behaviour of the EAKF-RN with small β values. As one can see in Figs. 5 and 6, given different filter configurations, the EAKF-RN may behave quite differently at relatively large β values. However, as β tends to 0, the time mean RMSEs of the EAKF-RN with different configurations tend to converge, despite the different combinations of l_c and λ . This is because, as $\beta \rightarrow 0$,

$c_k \rightarrow 0$ in Eq. (8), hence the new estimate $\tilde{\mathbf{x}}_k^a$, according to Eq. (9a), approaches the observation inversion \mathbf{x}_k^o , which is independent of, for instance, the half-width l_c , the inflation factor λ and the ensemble size⁵. Since the time mean RMSE continuously depends on β , it is not surprising to find that in Figs. 5 and 6, the time mean RMSEs of the EAKF-RN with small β , say at $\beta = 0.02$, are very close to the corresponding values at $\beta = 0$.

More insights of the filters' behaviour may be gained by examining the fraction coefficient c_k in the EAKF-RN. For the relatively good filter configuration ($l_c = 0.1$ and $\lambda = 1.15$), we have seen in Fig. 5 that the EAKF and the EAKF-RN have very close performance, and our experiment results show that c_k mostly concentrate on 1, similar to the situations on the lower panels of Fig. 2 (not reported). Of more interest is the case in which the normal EAKF is less properly configured ($l_c = 0.3$ and $\lambda = 1.05$), and may suffer from filter divergence. On the upper panels of Fig. 7 we show sample time series of the RMSEs of the normal EAKF and EAKF-RN ($\beta = 2$) in the 1/2 observation scenario. On the upper left panel, the EAKF has an exceptionally large RMSE (in the order of 10^{21}) at time step $k = 26$, is thus considered diverged. In contrast, on the upper right panel, the EAKF-RN ($\beta = 2$) has all the RMSEs less than 5 (with the corresponding time mean RMSE being 1.8931), and filter divergence is avoided. The lower left panel shows the time series of the fraction coefficient c_k , which has the mean 0.9499 and the median 1. Among 250 c_k values, 78 are less than 1. For reference, a histogram of c_k is plotted on the lower right panel, which confirms that c_k largely concentrate on 1.

In Fig. 8 we also examine what happens before the normal EAKF diverges. On the upper panel, we show the time series of the RMSEs of the EAKF (in the solid line with asterisks) and the EAKF-RN ($\beta = 2$, in the dotted line with plus signs). One can see that, at the beginning, say, when the time instant $k \leq 15$, the difference between the EAKF and the EAKF-RN is relatively less significant. For $16 \leq k \leq 25$, the difference becomes more obvious. On the middle panel we report the difference between the EAKF and the EAKF-RN ($\beta = 2$), in terms of the RMSE of the EAKF minus that of the EAKF-RN, for $1 \leq k \leq 16$. The reason for not including the RMSE differences at larger time instants is that their amplitudes are relatively large and may make relatively small values indistinguishable from 0, which is not desired for our purpose. On the lower panel, we also show the fraction coefficients c_k of the EAKF-RN ($\beta = 2$) for $1 \leq k \leq 25$. Note the availability of c_k depends on the availability of the incoming observations, therefore c_k appear for every 4 steps only. Based on these figures, one may tell what happens to make the EAKF and EAKF-RN behave differently. At time step $k = 4$, there is an incoming observation. However, because $c_4 = 1$, the EAKF and EAKF-RN share identical estimates from $k = 1$ to $k = 7$. At $k = 8$, there is one more incoming observation, and this time c_8 is less than 1, meaning that residual nudging is effective, so that there is a (very) small difference spotted between the estimates

of the EAKF and EAKF-RN. At $k = 12$, residual nudging is conducted again (but no more for subsequent steps up to $k = 24$), which, together with the previous residual nudging, makes the estimates of the EAKF-RN deviate from those of the EAKF, and eventually avoid filter divergence at $k = 26$.

Overall, we have shown that, when the normal EAKF is properly configured, the performance of the normal EAKF and the EAKF-RN is in general comparable. However, if the EAKF is not configured properly, then the EAKF-RN may perform (substantially) better than the normal EAKF. For many large scale data assimilation problems, it may be very expensive to conduct an extensive parameter searching in order to configure the EnKF (Anderson, 2007). Should the EnKF be ill-configured, we expect that introducing residual nudging to the EnKF may enhance its performance, in terms of filter accuracy and/or stability against divergence.

4.2.3 Results with different ensemble sizes Here we examine the effect of the ensemble size n on the performance of the normal EAKF and the EAKF-RN. The experiment settings are as follows. We also conduct the experiment in four observation scenarios. The ensemble size n is chosen from the set $\{2, 4, 6, 8, 10, 20, 40, 60, 80\}$. In the experiment we fix $l_c = 0.1$ and $\lambda = 1.15$ for both the normal EAKF and the EAKF-RN. In the EAKF-RN, we adopt two noise level coefficients, with β being 1 and 2, respectively.

Fig. 9 shows the time mean RMSEs of the normal EAKF (solid lines with squares), and those of the EAKF-RNs with $\beta = 1$ and 2 (dotted lines with bold points, and dash-dotted lines with crosses, respectively), in different observation scenarios. In the full observation scenario, no filter divergence is found for all the ensemble sizes n in either filter. When $n \leq 10$, the EAKF-RN with $\beta = 1$ tends to perform better than the EAKF-RN with $\beta = 2$, while the latter is better than the normal EAKF. This is particularly the case with a relatively small ensemble size, say at $n = 2$. On the other hand, when $n \geq 20$, the time mean RMSEs of the three filters are almost indistinguishable.

In the 1/2 observation scenario, the normal EAKF diverges when $n \leq 10$, so there are no square markers appearing at those n values. The EAKF-RN with $\beta = 2$ appears more robust than the normal EAKF, although there is still a filter divergence spotted at $n = 4$. In contrast, the EAKF-RN with $\beta = 1$ is the most robust filter, which does not diverge for all the tested ensemble sizes. In terms of time mean RMSE, though, when the filters do not diverge, the EAKF-RN with $\beta = 1$ tends to perform worse than the EAKF-RN with $\beta = 2$, while the latter appears to be indistinguishable from the normal EAKF for $n \geq 20$.

The situations in the 1/4 and 1/8 observation scenarios are similar to that in the 1/2 one. In the 1/4 observation scenario, the normal EAKF diverges for $n \leq 8$, while the EAKF-RN appears to be more robust, except that there is a filter divergence at $n = 4$ for the EAKF-RN with $\beta = 2$. When $n = 2$, the EAKF-RN with $\beta = 2$ performs better than the filter with $\beta = 1$, but at $n = 6$ or 8, the filter with $\beta = 1$ performs better instead. For $n \geq 10$, the performance of all three filters are almost indistinguishable. In the 1/8 observation scenario, the normal EAKF and the EAKF-RN with $\beta = 2$ diverge at $n = 2$ and 4, while the EAKF-RN with $\beta = 1$ diverges only at $n = 2$. For $n = 6$ or 8, the EAKF-

⁵ When the observation operator is time-varying, the assimilation step S_a in general has an influence on the observation inversion, as S_a decides when the observations are assimilated.

971 RN with $\beta = 1$ has the best performance in terms of time 1031
 972 mean RMSE, the EAKF-RN with $\beta = 2$ the second, while 1032
 973 the normal EAKF the last. For $n \geq 10$, the performance of 1033
 974 the three filters are almost indistinguishable, except that at 1034
 975 $n = 10$, the time mean RMSE of the EAKF-RN with $\beta = 1$ 1035
 976 is slightly higher than those of the other two filters.

977 The above results suggest that $n = 20$ appears to be a 1036
 978 reasonable ensemble size for the normal EAKF in the L96 1037
 979 model, since in all these four observation scenarios, the per- 1038
 980 formance of the normal EAKF with $n = 20$ is very close to 1039
 981 that with larger n values. As the ensemble size n decreases, 1040
 982 the normal EAKF becomes more unstable. The performance 1041
 983 of the EAKF-RN with $\beta = 1$ and 2 is almost indistinguish- 1042
 984 able from the normal EAKF for $n \geq 20$. However, given 1043
 985 smaller ensemble sizes, the EAKF-RN tends to perform bet- 1044
 986 ter than the normal EAKF, in terms of both filter accuracy 1045
 987 and stability against filter divergence. In particular, one may 1046
 988 enhance the stability of the EAKF-RN by reducing the noise 1047
 989 level coefficient β , since as $\beta \rightarrow 0$, the time mean RMSEs 1048
 990 of the EAKF-RN in different observation scenarios become 1049
 991 independent of the ensemble size n , and approach the corre- 1050
 992 sponding values at $\beta = 0$. This property may be of interest 1051
 993 in certain circumstances, for instance, those in which, due 1052
 994 to practical limitations, one can only afford to run an EnKF 1053
 995 with a very small ensemble size, so that filter stability be- 1054
 996 comes an important factor in consideration. 1055

997 *4.2.4 Results with different assimilation steps and obser-* 1056
 998 *vation noise variances* Here we examine the effects of the 1057
 999 assimilation step S_a and the observation noise variance on 1058
 1000 the performance of the normal EAKF and the EAKF-RN. 1059
 1001 We assume that the observation noise covariance matrix \mathbf{R}_k 1060
 1002 is in the form of $\gamma \mathbf{I}$, where \mathbf{I} is the identity matrix with a suit- 1061
 1003 able dimension in different observation scenarios, and $\gamma > 0$ 1062
 1004 is a real scalar. As a result, the variances of \mathbf{R}_k are γ for all 1063
 1005 variables in an observation vector, while the cross-variances 1064
 1006 are all zero. The experiment settings are the following. The 1065
 1007 ensemble size is 20, $l_c = 0.1$ and $\lambda = 1.15$ for both the 1066
 1008 normal EAKF and the EAKF-RN. The noise level coeffi- 1067
 1009 cients β is 2 in the EAKF-RN. We conduct the experiment 1068
 1010 in four different observation scenarios, and choose S_a from 1069
 1011 the set $\{1, 4, 8, 12\}$, and γ from the set $\{0.01, 0.1, 1, 10, 50\}$. 1070
 1012 The relatively large values of γ , say $\gamma = 10, 50$, are used to 1071
 1013 represent the scenario in which the quality of the observa- 1072
 1014 tions is relatively poor. Here we assume that we know the 1073
 1015 observation noise variance precisely, while in a subsequent 1074
 1016 experiment we will consider the case in which the observa- 1075
 1017 tion noise variance is mis-specified. 1076
 1018

1019 Figs. 10 and 11 show the time mean RMSEs of the 1077
 1020 normal EAKF and the EAKF-RN, respectively, in different 1078
 1021 observation scenarios. In the full observation scenario (upper 1079
 1022 left panels), for a fixed variance γ , the time mean RMSEs of 1080
 1023 both the normal EAKF and the EAKF-RN tend to increase 1081
 1024 as the assimilation step S_a increases. On the other hand, 1082
 1025 for a fixed S_a , the time mean RMSEs of both filters appear 1083
 1026 to be monotonically increasing functions of the variance γ . 1084
 1027 With $\gamma = 0.01, 0.1, 1$, the time mean RMSEs of the EAKF- 1085
 1028 RN tend to be lower than those of the normal EAKF, while 1086
 1029 with $\gamma = 10, 50$, they are almost indistinguishable, meaning 1087
 1030 that for relatively poor observation, the normal EAKF and 1088
 the EAKF-RN have almost the same performance in terms 1089
 1090

of estimation accuracy, which appears to be also true in 1091
 other observation scenarios, as will be shown below. In terms 1092
 of filter stability, for $S_a = 8$ and 12, the normal EAKF 1093
 diverges at $\gamma = 0.01$ and 0.1, but the EAKF-RN avoids 1094
 filter divergences at all these places.

In the 1/2 observation scenario (upper right panels), for 1095
 a fixed variance γ , the time mean RMSEs of both the nor- 1096
 mal EAKF and the EAKF-RN also grow as the assimilation 1097
 step S_a increases. However, for a fixed S_a , the time mean 1098
 RMSEs of the two filters have behaviour different from that 1099
 in the previous observation scenario. For $S_a = 1$, the time 1100
 mean RMSE of the normal EAKF is still a monotonically 1101
 increasing function of γ ; for $S_a = 4, 8$, the normal EAKF 1102
 diverges at $\gamma = 0.01$ and 0.1, and has monotonically in- 1103
 creasing time mean RMSE for $\gamma \geq 1$; for $S_a = 12$, the time 1104
 mean RMSE of the normal EAKF achieves its minimum at 1105
 $\gamma = 0.1$ (slightly lower than that at 0.01), and thus exhibits 1106
 the U-turn behaviour, a phenomenon that is more visible 1107
 in the EAKF-RN. Indeed, for all tested S_a values, the time 1108
 mean RMSEs of the EAKF-RN all have their minima at 1109
 $\gamma = 0.1$, rather than at $\gamma = 0.01$. The normal EAKF and the 1110
 EAKF-RN have almost indistinguishable time mean RM- 1111
 SEs for $\gamma \geq 1$. While the normal EAKF tends to perform 1112
 better than the EAKF-RN at $\gamma = 0.01$ and 0.1 in terms 1113
 of time mean RMSE, it is more likely to suffer from filter 1114
 divergence (e.g., at $S_a = 4, 8$). This is an example of the 1115
 trade-off between filter accuracy and stability, as discussed 1116
 in §2.3.

In the 1/4 observation scenario (lower left panels), for 1117
 a fixed assimilation step S_a , the time mean RMSEs of both 1118
 the normal EAKF and the EAKF-RN again appear to be 1119
 monotonically increasing as γ increases. For a fixed variance 1120
 γ , though, the time mean RMSEs of both filters tend to 1121
 exhibit the U-turn behaviour, in which the minimum time 1122
 mean RMSE is achieved at $S_a = 4$ (except for the filter 1123
 divergence in the normal EAKF at $\gamma = 0.01$), rather than 1124
 at $S_a = 1$. The normal EAKF and the EAKF-RN have 1125
 almost indistinguishable time mean RMSEs for $\gamma \geq 0.1$. 1126
 At $\gamma = 0.01$, though, the normal EAKF seems to perform 1127
 better than the EAKF-RN in terms of time mean RMSE. 1128
 However, filter divergences are spotted at ($S_a = 4, \gamma = 0.01$) 1129
 and ($S_a = 1, \gamma = 50$), which are again avoided in the EAKF- 1130
 RN.

In the 1/8 observation scenario (lower right panels), the 1131
 quantitative behaviour of the two filters, as functions of S_a 1132
 and γ , is almost the same as that in the 1/4 observation sce- 1133
 nario. The main differences are the following. The time mean 1134
 RMSEs of the normal EAKF and the EAKF-RN are almost 1135
 indistinguishable in all tested cases. Filter divergences are 1136
 spotted at $S_a = 1$, with $\gamma = 1, 10$ and 50, respectively, not 1137
 only in the normal EAKF, but also in the EAKF-RN. One 1138
 may, however, avoid these filter divergences in the EAKF- 1139
 RN by assigning to it a smaller β , as some of the previous 1140
 experiment results have suggested.

Overall, the above experiment results are consistent 1141
 with our discussion in § 2.3. When equipped with residual 1142
 nudging, the EAKF-RN appears to be more stable than the 1143
 normal EAKF, although maybe at the cost of some loss of es- 1144
 timation accuracy in certain circumstances (e.g., when with 1145
 too small β values).

1091 *4.2.5 Results with imperfect models and mis-specified ob-*
 1092 *servations error covariances* Finally, we examine filter per- 1148
 1093 formance of the normal EAKF and the EAKF-RN when 1149
 1094 they are subject to uncertainties in specifying the forcing 1150
 1095 term F in Eq. (15) and the observation error covariance 1151
 1096 \mathbf{R}_k . We again conduct the experiments in four observation 1152
 1097 scenarios. The ensemble sizes of both filters are 20. The half- 1153
 1098 width l_c of covariance localization is 0.1, and the covariance 1154
 1099 inflation factor λ is 1.15. The true value of F is 8, while 1155
 1100 the true observation error covariance \mathbf{R}_k is \mathbf{I}_{20} . In the ex- 1156
 1101 periments we let the value of F in the (possibly) imperfect 1157
 1102 model be chosen from the set $\{4, 6, 8, 10, 12\}$, and the (pos- 1158
 1103 sibly) mis-specified covariance \mathbf{R}_k in the form of $\gamma\mathbf{I}_{20}$, with 1159
 1104 $\gamma \in \{0.25, 0.5, 1, 2, 5, 10\}$ ⁶. In the EAKF-RN the noise level 1160
 1105 coefficient $\beta = 2$. 1161

1162 Figs. 12 and 13 show the time mean RMSEs of the normal 1163
 1164 EAKF and the EAKF-RN, respectively, as functions of the 1164
 1165 (possibly) mis-specified driving force F and the obser- 1165
 1166 vation noise variance γ , in different observation scenarios. 1166
 1167 In the full observation scenario (upper left panels), for a 1167
 1168 fixed γ , the time mean RMSEs of both filters exhibit the 1168
 1169 U-turn behaviour with respect to F , achieving their minima 1169
 1170 at $F = 8$. This point also appears to be valid in other obser- 1170
 1171 vation scenarios. On the other hand, for a fixed F , the 1171
 1172 behaviour of the filters is very similar to that reported in 1172
 1173 Figs. 5 and 6, since the role of the (possibly) mis-specified 1173
 1174 variance γ is similar to the observation noise level coeffi- 1174
 1175 cient β (note, though, that γ also appears in the computa- 1175
 1176 tion of the Kalman gain). When γ is relatively small (say 1176
 1177 $\gamma \leq 2$), the EAKF-RN tends to perform better than the 1177
 1178 normal EAKF in terms of time mean RMSE. Moreover, the 1178
 1179 normal EAKF diverges at ($F = 12, \gamma = 0.25$), while the 1179
 1180 EAKF-RN avoids the divergence. On the other hand, when 1180
 1181 γ is relatively large (say $\gamma \geq 6$), the EAKF-RN and the nor- 1181
 1182 mal EAKF have almost indistinguishable performance, not 1182
 1183 only for the current experiment results, but also for those in 1183
 1184 the other observation scenarios. This is largely because mis- 1184
 1185 takenly over-estimating the variance γ has an effect similar 1185
 1186 to increasing β , so that the observation inversion in Eq. (9a) 1186
 1187 becomes less influential for state estimation, and the EAKF- 1187
 1188 RN has almost the same estimate as the normal EAKF. 1188

1189 In the 1/2 observation scenario (upper right panels), 1189
 1190 when γ is relatively small (say $\gamma \leq 1$), the normal EAKF 1190
 1191 tends to diverge for all F . The EAKF-RN avoids filter diver- 1191
 1192 gences in some of the areas, though there are still two cases 1192
 1193 spotted at $F = 12$, with $\gamma = 1$ and $\gamma = 2$, respectively. As 1193
 1194 γ becomes larger, the performance of the normal EAKF and 1194
 1195 the EAKF-RN are very close to each other, similar to the 1195
 1196 situation in the full observation scenario. In both the 1/4 1196
 1197 and 1/8 observation scenarios (lower panels), there are also 1197
 1198 almost no differences between the time mean RMSEs of the 1198
 1199 two filters, although the time mean RMSE of the EAKF-RN 1199
 1200 appears to be slightly lower than that of the normal EAKF 1200
 1201 in the 1/4 observation scenario for relatively small F and γ 1201
 1202 (around the lower left corners). Both filters diverge in the 1202
 1203 1/4 observation scenario, at ($F = 10, \gamma = 0.25$), otherwise 1203
 1204 neither filter diverges. 1204
 1205

⁶ The (possibly) mis-specified observation error covariance, in the form of $\gamma\mathbf{I}_{20}$, is used for both background update, as described in §2.1, and residual nudging through Eq. (8).

1148 5 Discussion and conclusion

In this work we proposed an auxiliary technique, called residual nudging, for ensemble Kalman filtering. The main idea of residual nudging is to monitor, and if necessary, adjust the residual norm of a state estimate. In an under-determined state estimation problem, if the residual norm is larger than a pre-specified value, then we reject the estimate and replace it by a new one whose residual norm is equal to the pre-specified value; otherwise we accept the estimate. We discussed how to choose the pre-specified value, and demonstrated how one can construct a new state estimate based on the original one and the observation inversion, given a linear observation operator.

Through the numerical experiments in both the scalar AR1 and the Lorenz 96 models, we showed that, by choosing a proper noise level coefficient, the ensemble adjustment Kalman filter with residual nudging (EAKF-RN) in general works more stably than the normal EAKF, while achieving an accuracy that is often comparable to, sometime even (much) better than that of the normal EAKF, especially if the normal EAKF is ill-configured. This may occur, for instance, when the EAKF is equipped with improperly chosen covariance inflation factor and/or half-width of covariance localization, too small ensemble size, and so on. In many data assimilation practices, it may be very expensive to conduct extensive searching for proper inflation factor and/or half-width, or to run a large scale model with too many ensemble members. In such circumstances, we expect that residual nudging may help improve the filter performance, in terms of filter stability, and even accuracy.

We also implemented residual nudging in some other filters, including the stochastic ensemble Kalman filter (Burgers et al., 1998) and the singular evolutive interpolated Kalman filter (SEIK) (Hoteit et al., 2002; Pham, 2001), and observed similar performance improvements (not shown in this work). Since residual nudging only aims to adjust the estimates, we envision that residual nudging can be associated with other data assimilation approaches, including, for instance, the extended Kalman filter, the particle filter, and various smoothers. This will be verified elsewhere.

One problem not addressed in this work is the nonlinearity of the observation operator. In such circumstances, we conjecture that the rule in choosing the pre-specified value $\beta\sqrt{\text{trace}(\mathbf{R}_k)}$ may still be applicable. However, the construction of new state estimates would become more complicated than Eqs. (8) and (9). One possible strategy is to linearize the observation operator, or employ more sophisticated methods, such as iterative searching algorithms (see, for example, Gu and Oliver 2007; Lorentzen and Nævdal 2011), to find new estimates whose residual norms are no larger than $\beta\sqrt{\text{trace}(\mathbf{R}_k)}$. This is another topic that will be investigated in the future.

1200 Acknowledgement

1201 We thank Dr Jeffrey Anderson for his kind advices on
 1202 using the EAKF codes (MATLAB) in the Data Assimilation
 1203 Research Testbed (DART, version "kodiak", 2011).
 1204 This provides the basis for us to build the EAKF codes used
 1205 in our experiments.

We also thank two anonymous reviewers for their constructive comments and suggestions. One reviewer points out the similarity between residual nudging and the adaptive inflation schemes in Anderson (2007; 2009), and suggests conducting the experiment with respect to the KF in the AR1 model. Another reviewer points out the possible combinations of the EnKF and the regularization approaches in inverse problems.

Luo acknowledges partial financial support from the Research Council of Norway and industrial partners, through the project "Transient well flow modelling and modern estimation techniques for accurate production allocation".

REFERENCES

- Anderson, J. L. 2001. An ensemble adjustment Kalman filter for data assimilation. *Mon. Wea. Rev.* **129**, 2884–2903.
- Anderson, J. L. 2007. An adaptive covariance inflation error correction algorithm for ensemble filters. *Tellus* **59A**(2), 210–224.
- Anderson, J. L. 2009. Spatially and temporally varying adaptive covariance inflation for ensemble filters. *Tellus* **61A**, 72–83.
- Anderson, J. L. and Anderson, S. L. 1999. A Monte Carlo implementation of the nonlinear filtering problem to produce ensemble assimilations and forecasts. *Mon. Wea. Rev.* **127**, 2741–2758.
- Bishop, C. H., Etherton, B. J. and Majumdar, S. J. 2001. Adaptive sampling with ensemble transform Kalman filter. Part I: theoretical aspects. *Mon. Wea. Rev.* **129**, 420–436.
- Burgers, G., van Leeuwen, P. J. and Evensen, G. 1998. On the analysis scheme in the ensemble Kalman filter. *Mon. Wea. Rev.* **126**, 1719–1724.
- Engl, H. W., Hanke, M. and Neubauer, A. 2000. Regularization of inverse problems Engl, H. W., Hanke, M. and Neubauer, A. Springer.
- Evensen, G. 1994. Sequential data assimilation with a nonlinear quasi-geostrophic model using Monte Carlo methods to forecast error statistics. *J. Geophys. Res.* **99**, 10143–10162.
- Fertig, E., Harlim, J. and Hunt, B. 2007. A comparative study of 4D-VAR and a 4D ensemble Kalman filter: perfect model simulations with lorenz-96. *Tellus A* **59**, 96–100.
- Gandin, L. S. 1988. Complex quality control of meteorological observations. *Mon. Wea. Rev.* **116**, 1137–1156.
- Gaspari, G. and Cohn, S. E. 1999. Construction of correlation functions in two and three dimensions. *Quart. J. Roy. Meteor. Soc.* **125**, 723 – 757.
- Gu, Y. and Oliver, D. 2007. An iterative ensemble Kalman filter for multiphase fluid flow data assimilation. *SPE Journal* **12**, 438–446.
- Hamill, T. M., Whitaker, J. S., Anderson, J. L. and Snyder, C. 2009. Comments on "Sigma-point Kalman filter data assimilation methods for strongly nonlinear systems". *J. Atmos. Sci.* **66**, 3498–3500.
- Hamill, T. M., Whitaker, J. S. and Snyder, C. 2001. Distance-dependent filtering of background error covariance estimates in an ensemble Kalman filter. *Mon. Wea. Rev.* **129**, 2776–2790.
- Hoteit, I., Pham, D. T. and Blum, J. 2002. A simplified reduced order Kalman filtering and application to altimetric data assimilation in Tropical Pacific. *Journal of Marine Systems* **36**, 101–127.
- Houtekamer, P. L. and Mitchell, H. L. 1998. Data assimilation using an ensemble Kalman filter technique. *Mon. Wea. Rev.* **126**, 796–811.
- Hunt, B., Kalnay, E., Kostelich, E., Ott, E., Patil, D., Sauer, T., Szunyogh, I., Yorke, J. and Zimin, A. 2004. Four-dimensional ensemble kalman filtering. *Tellus A* **56**(4), 273–277.
- Jazwinski, A. H. 1970. Stochastic processes and filtering theory Jazwinski, A. H. Academic Press.
- Kalman, R. 1960. A new approach to linear filtering and prediction problems. *Trans. ASME, Ser. D, J. Basic Eng.* **82**, 35–45.
- Lorentzen, R. and Nævdal, G. 2011. An iterative ensemble Kalman filter. *IEEE Transactions on Automatic Control* **56**, 1990–1995.
- Lorenz, E. N.: 1996, Predictability—a problem partly solved, in T. Palmer (ed.), *Predictability*, ECMWF, Reading, UK, pp. 1–18.
- Lorenz, E. N. and Emanuel, K. A. 1998. Optimal sites for supplementary weather observations: Simulation with a small model. *J. Atmos. Sci.* **55**, 399–414.
- Luo, X. and Hoteit, I. 2011. Robust ensemble filtering and its relation to covariance inflation in the ensemble Kalman filter. *Mon. Wea. Rev.* **139**, 3938–3953.
- Meyer, C. D. 2001. Matrix analysis and applied linear algebra Meyer, C. D. SI.
- Pham, D. T. 2001. Stochastic methods for sequential data assimilation in strongly nonlinear systems. *Mon. Wea. Rev.* **129**, 1194–1207.
- Sacher, W. and Bartello, P. 2008. Sampling errors in ensemble Kalman filtering. Part I: Theory. *Mon. Wea. Rev.* **136**(8), 3035–3049.
- Schlee, F. H., Standish, C. J. and Toda, N. F. 1967. Divergence in the kalman filter. *AIAA Journal* **5**, 1114–1120.
- Song, H., Hoteit, I., Cornuelle, B. and Subramanian, A. 2010. An adaptive approach to mitigate background covariance limitations in the ensemble Kalman filter. *Mon. Wea. Rev.* **138**(7), 2825–2845.
- Van Leeuwen, P. J. 2010. Nonlinear data assimilation in geosciences: an extremely efficient particle filter. *Quart. J. Roy. Meteor. Soc.* **136**, 1991–1999.
- Whitaker, J. S. and Hamill, T. M. 2002. Ensemble data assimilation without perturbed observations. *Mon. Wea. Rev.* **130**, 1913–1924.

1306 **LIST OF TABLES**

- 1307 1 Time mean RMSEs and spreads of the KF, and the minimum time mean RMSEs (over different β) of the
1308 KF-RN, in the AR1 model with different S_a . The KF and KF-RN have identical time mean spreads, therefore only
1309 those of the KF are presented. In the bottom row we also report the ranges of β in which the minimum time mean
1310 RMSEs of the KF-RN are achieved.
- 1311 2 Time mean RMSEs (spreads) of the normal EAKF and the EAKF-RN in the 1/2 observation scenario, as
1312 functions of the covariance inflation factor and the half-width of covariance localization.
- 1313 3 As in Table 2, except that it is in the 1/4 observation scenario.

1314 **LIST OF FIGURES**

- 1315 1 Time mean RMSEs of the KF and the KF-RN as functions of the noise level coefficient in the AR1 model, with
 1316 different S_a .
- 1317 2 Left panels: Sample time series of the fraction coefficients of the KF-RN with $\beta = 0.1$ (upper) and $\beta = 1$
 1318 (lower), respectively. Right panels: The corresponding histograms of the fraction coefficient time series.
- 1319 3 Time mean RMSEs of the normal EAKF and the EAKF-RN, as functions of inflation factor and half-width,
 1320 in the full and 1/8 observation scenarios.
- 1321 4 Time mean spreads of the normal EAKF and the EAKF-RN, as functions of inflation factor and half-width, in
 1322 the full and 1/8 observation scenarios.
- 1323 5 Time mean RMSEs of the normal EAKF and the EAKF-RN as functions of the noise level coefficient in different
 1324 observation scenarios, with $\lambda = 1.15$ and $l_c = 0.1$.
- 1325 6 As in Fig. 5, but with $\lambda = 1.05$ and $l_c = 0.3$ for both the filters. Note that in the 1/2 and 1/4 observation
 1326 scenarios divergences of the normal EAKF are spotted, hence no horizontal lines are indicated in the corresponding
 1327 plots. The EAKF-RN also diverges in the 1/2 and 1/4 observation scenarios for $\beta \geq 4$.
- 1328 7 Upper left: sample time series of the RMSE of the normal EAKF in the 1/2 observation scenario; Upper right:
 1329 sample time series of the RMSE of the EAKF-RN ($\beta = 2$) under the same experiment settings as the EAKF; Lower
 1330 left: corresponding fraction coefficient c_k in the EAKF-RN ($\beta = 2$); Lower right: corresponding histogram of c_k .
- 1331 8 Upper: the RMSE of the EAKF (solid line with asterisks) and EAKF-RN ($\beta = 2$, dotted line with plus signs)
 1332 between the time instant $k = 1$ and $k = 25$; Middle: difference in the RMSE (= RMSE of the EAKF - RMSE of
 1333 the EAKF-RN) between $k = 1$ and $k = 16$; Lower: the fraction coefficient of the EAKF-RN ($\beta = 2$) between $k = 1$
 1334 and $k = 25$.
- 1335 9 Time mean RMSEs of the EAKF and the EAKF-RN, as functions of the ensemble size in different observation
 1336 scenarios.
- 1337 10 Time mean RMSEs of the normal EAKF, as functions of the assimilation step S_a and the observation noise
 1338 variance, in different observation scenarios.
- 1339 11 As in Fig. 10, but for the EAKF-RN with $\beta = 2$.
- 1340 12 Time mean RMSEs of the EAKF, as functions of the (possibly) mis-specified driving force F and the observation
 1341 noise variance γ , in different observation scenarios.
- 1342 13 As in Fig. 12, but for the EAKF-RN with $\beta = 2$.

Table 1. Time mean RMSEs and spreads of the KF, and the minimum time mean RMSEs (over different β) of the KF-RN, in the AR1 model with different S_a . The KF and KF-RN have identical time mean spreads, therefore only those of the KF are presented. In the bottom row we also report the ranges of β in which the minimum time mean RMSEs of the KF-RN are achieved.

KF	$S_a =$			
	1	2	4	8
RMSE	0.6184	0.8260	1.0592	1.2997
spread	0.7729	1.0413	1.3419	1.8241
KF-RN	$S_a =$			
	1	2	4	8
min RMSE	0.6183	0.8259	1.0592	1.2997
achieved at	$\beta = 2$	$\beta = 2$	$\beta \geq 2$	$\beta \geq 2$

Table 2. Time mean RMSEs (spreads) of the normal EAKF and the EAKF-RN in the 1/2 observation scenario, as functions of the covariance inflation factor and the half-width of covariance localization.

EAKF	$l_c = 0.1$	$l_c = 0.2$	$l_c = 0.3$	$l_c = 0.4$	$l_c = 0.5$
$\lambda = 1.00$	1.0721 (0.7049)	Div	Div	Div	Div
$\lambda = 1.05$	1.0091 (0.7457)	Div	Div	Div	Div
$\lambda = 1.10$	0.9789 (0.7868)	Div	Div	Div	Div
$\lambda = 1.15$	0.9662 (0.8209)	Div	Div	Div	Div
$\lambda = 1.20$	0.9515 (0.8566)	Div	Div	Div	Div
$\lambda = 1.25$	0.9623 (0.8929)	Div	Div	Div	Div
EAKF-RN	$l_c = 0.1$	$l_c = 0.2$	$l_c = 0.3$	$l_c = 0.4$	$l_c = 0.5$
$\lambda = 1.00$	1.0325 (0.7002)	1.8256 (0.5697)	2.1099 (0.5127)	2.2734 (0.4736)	2.2964 (0.4579)
$\lambda = 1.05$	1.0051 (0.7419)	1.4072 (0.6185)	1.9879 (0.5644)	2.1821 (0.5269)	2.2468 (0.5050)
$\lambda = 1.10$	0.9598 (0.7842)	1.2313 (0.6553)	1.8517 (0.6030)	2.0342 (0.5699)	2.1742 (0.5470)
$\lambda = 1.15$	0.9673 (0.8201)	1.2024 (0.6870)	1.6507 (0.6388)	1.9317 (0.6015)	2.0953 (0.5845)
$\lambda = 1.20$	0.9474 (0.8565)	1.1788 (0.7183)	1.5776 (0.6680)	1.9059 (0.6336)	2.0806 (0.6098)
$\lambda = 1.25$	0.9650 (0.8935)	1.1856 (0.7484)	1.5315 (0.6945)	1.7778 (0.6603)	2.0071 (0.6383)

Table 3. As in Table 2, except that it is in the 1/4 observation scenario.

EAKF	$l_c = 0.1$	$l_c = 0.2$	$l_c = 0.3$	$l_c = 0.4$	$l_c = 0.5$
$\lambda = 1.00$	2.0685 (1.5730)	Div	Div	Div	Div
$\lambda = 1.05$	1.9908 (1.7849)	Div	Div	Div	Div
$\lambda = 1.10$	2.0223 (2.0447)	2.3014 (1.5640)	Div	Div	Div
$\lambda = 1.15$	2.0819 (2.3592)	2.2174 (1.7254)	2.9502 (1.5820)	Div	Div
$\lambda = 1.20$	2.1903 (2.6869)	2.1839 (1.9468)	2.7534 (1.7191)	Div	Div
$\lambda = 1.25$	2.3586 (3.0392)	2.2596 (2.2340)	2.6413 (1.8780)	Div	Div
EAKF-RN	$l_c = 0.1$	$l_c = 0.2$	$l_c = 0.3$	$l_c = 0.4$	$l_c = 0.5$
$\lambda = 1.00$	2.0840 (1.5689)	2.6099 (1.1984)	3.0267 (1.0110)	3.0453 (0.8703)	3.0469 (0.7899)
$\lambda = 1.05$	2.0042 (1.7790)	2.3341 (1.3762)	2.8493 (1.1936)	3.0573 (1.0403)	3.1015 (0.9618)
$\lambda = 1.10$	1.9860 (2.0339)	2.2976 (1.5332)	2.8154 (1.3484)	3.0527 (1.2112)	3.1251 (1.1028)
$\lambda = 1.15$	2.0766 (2.3648)	2.2389 (1.7244)	2.7737 (1.4940)	3.1247 (1.3341)	3.2583 (1.2558)
$\lambda = 1.20$	2.1886 (2.6948)	2.2312 (1.9710)	2.6566 (1.6824)	3.0992 (1.5048)	3.2340 (1.3674)
$\lambda = 1.25$	2.3436 (3.0359)	2.2352 (2.2344)	2.6168 (1.8427)	3.0977 (1.6509)	3.2897 (1.5098)

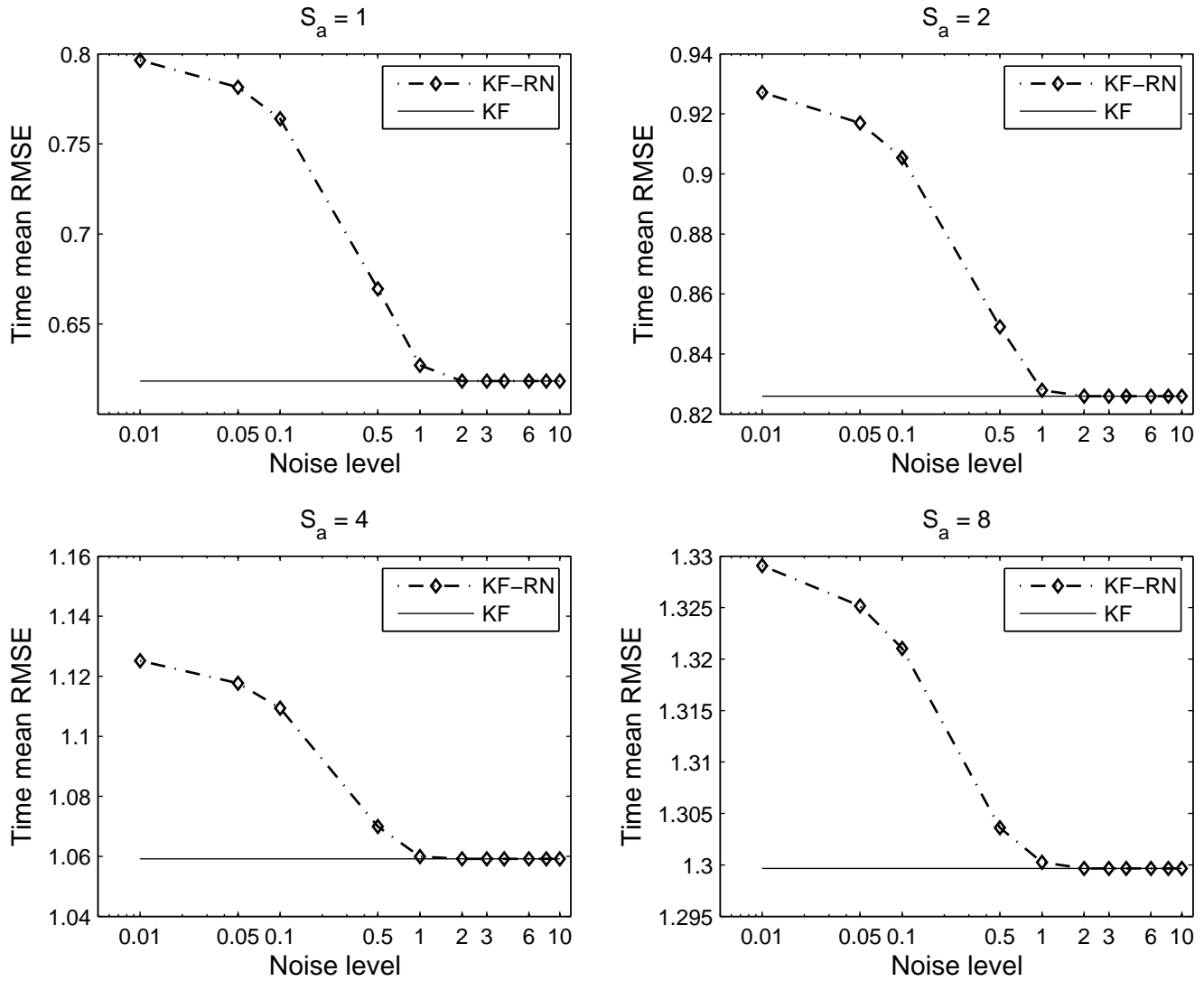


Figure 1. Time mean RMSEs of the KF and the KF-RN as functions of the noise level coefficient in the AR1 model, with different S_a .

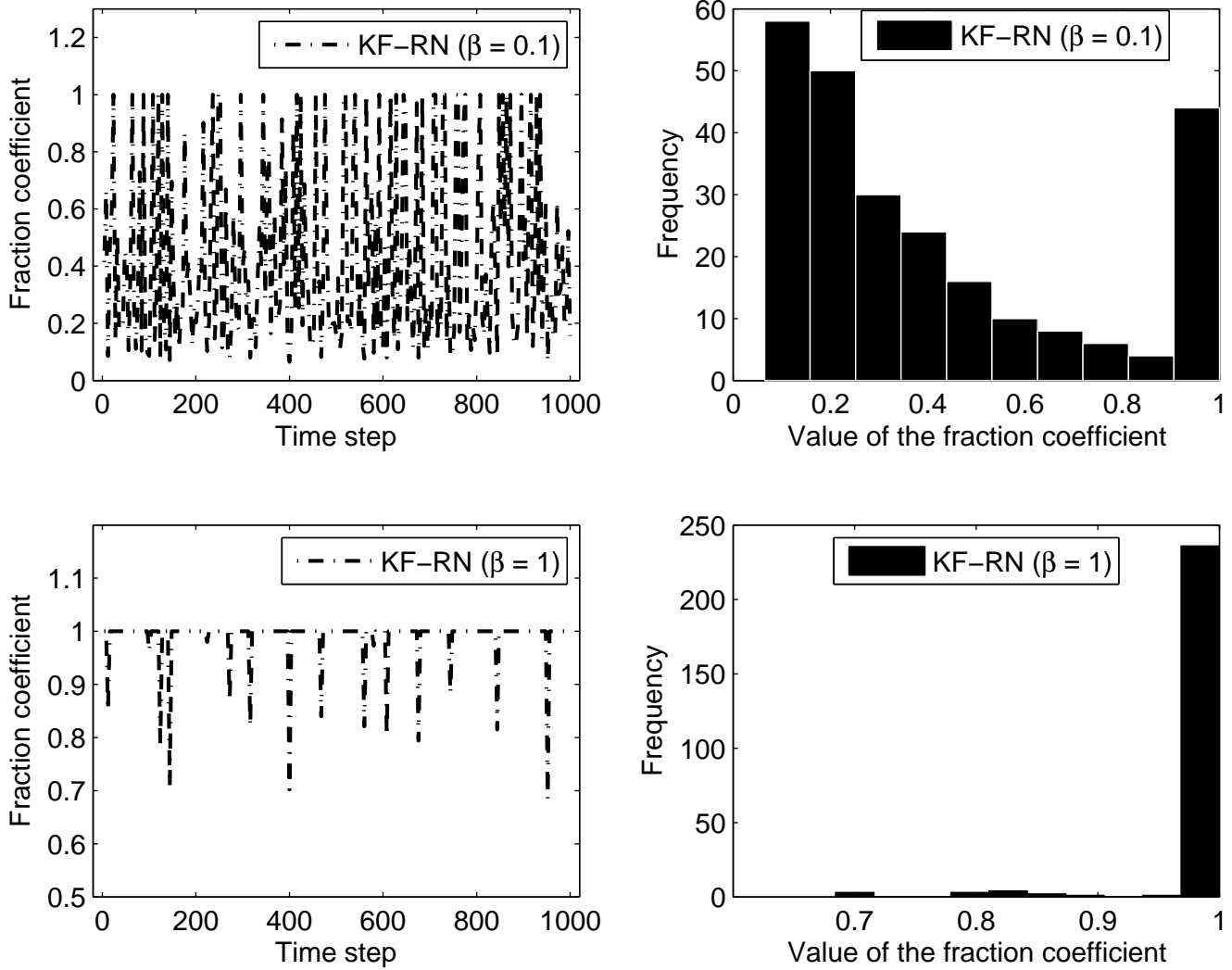


Figure 2. Left panels: Sample time series of the fraction coefficients of the KF-RN with $\beta = 0.1$ (upper) and $\beta = 1$ (lower), respectively. Right panels: The corresponding histograms of the fraction coefficient time series.

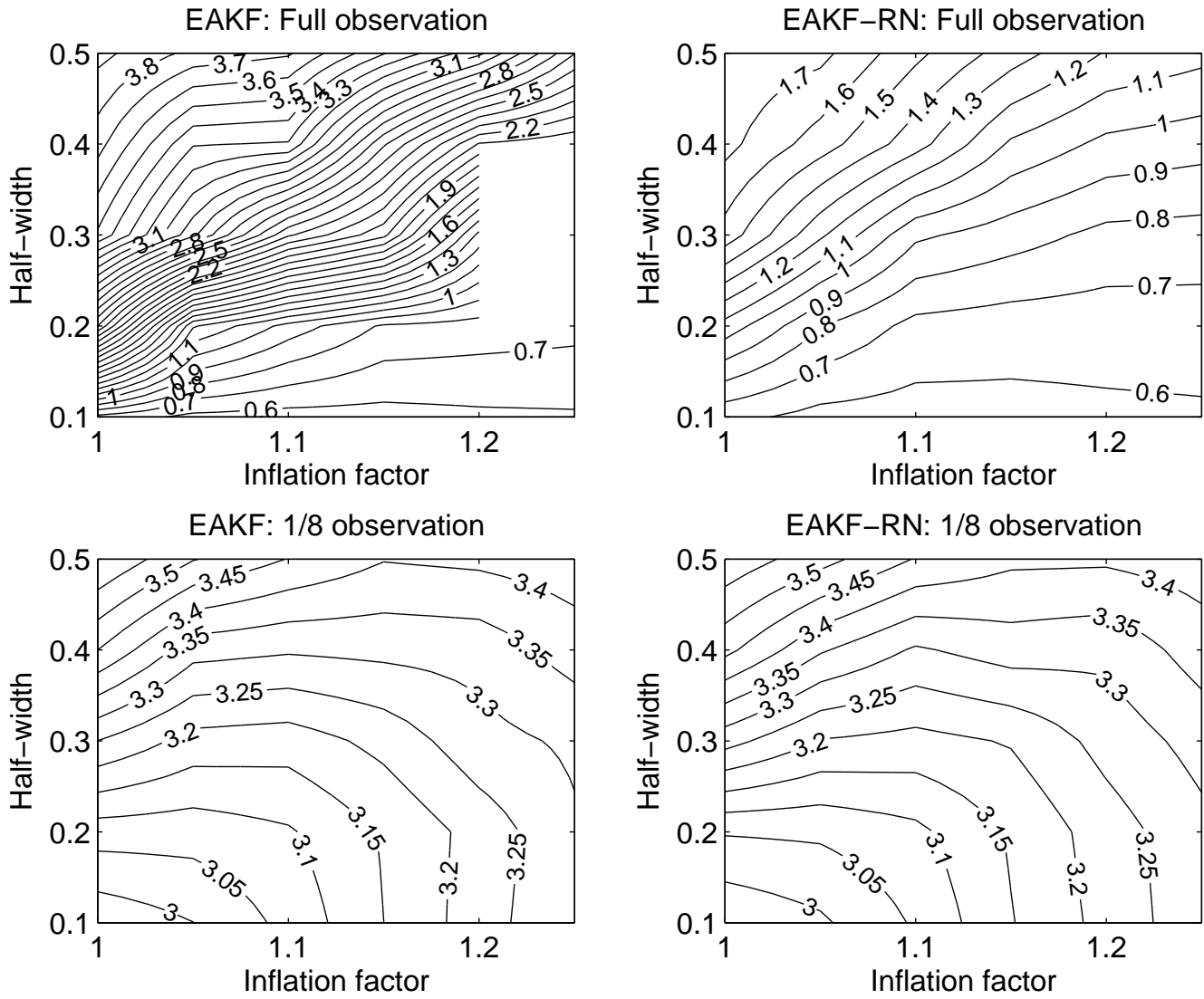


Figure 3. Time mean RMSEs of the normal EAKF and the EAKF-RN, as functions of inflation factor and half-width, in the full and 1/8 observation scenarios.

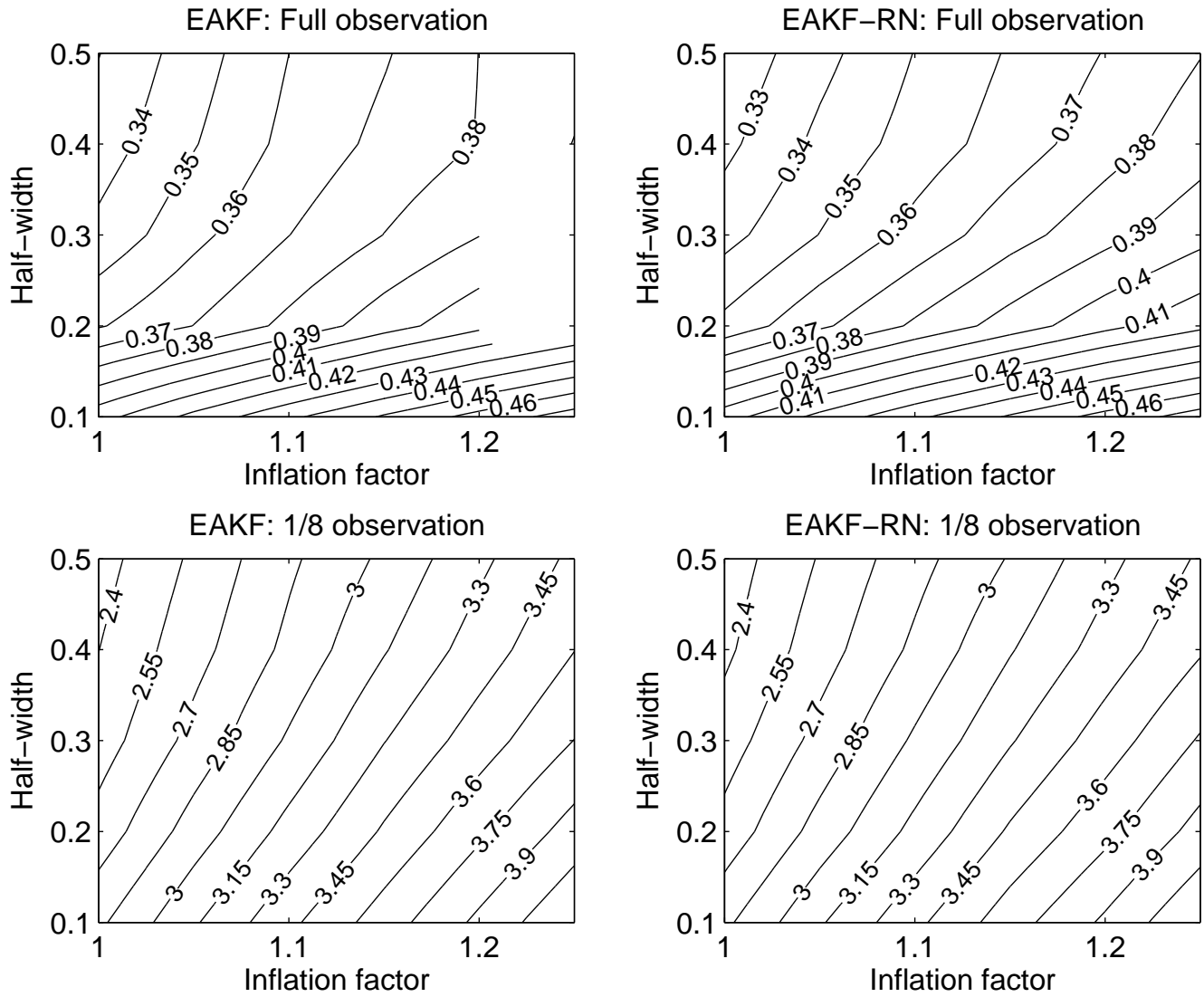


Figure 4. Time mean spreads of the normal EAKF and the EAKF-RN, as functions of inflation factor and half-width, in the full and 1/8 observation scenarios.

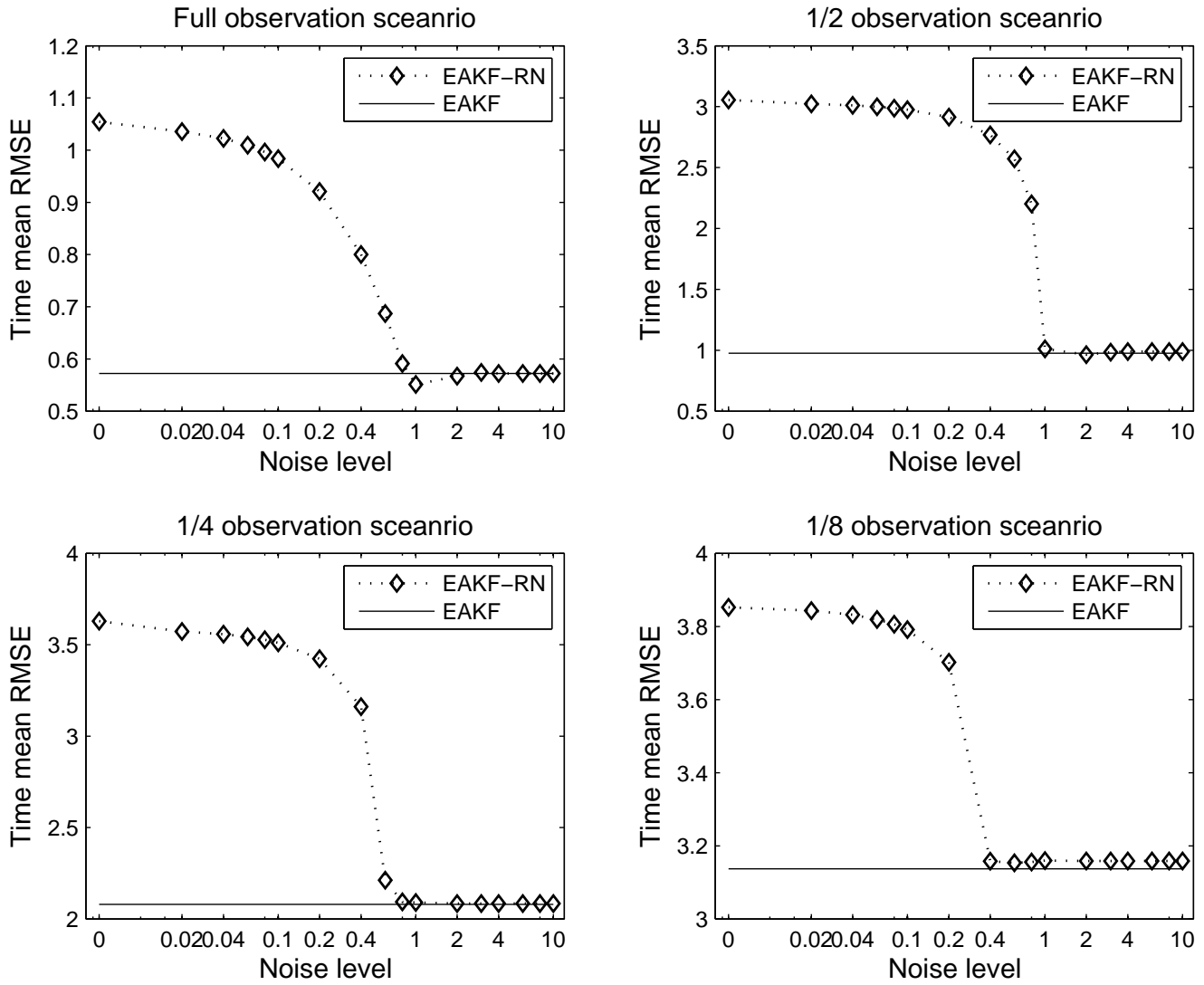


Figure 5. Time mean RMSEs of the normal EAKF and the EAKF-RN as functions of the noise level coefficient in different observation scenarios, with $\lambda = 1.15$ and $l_c = 0.1$.

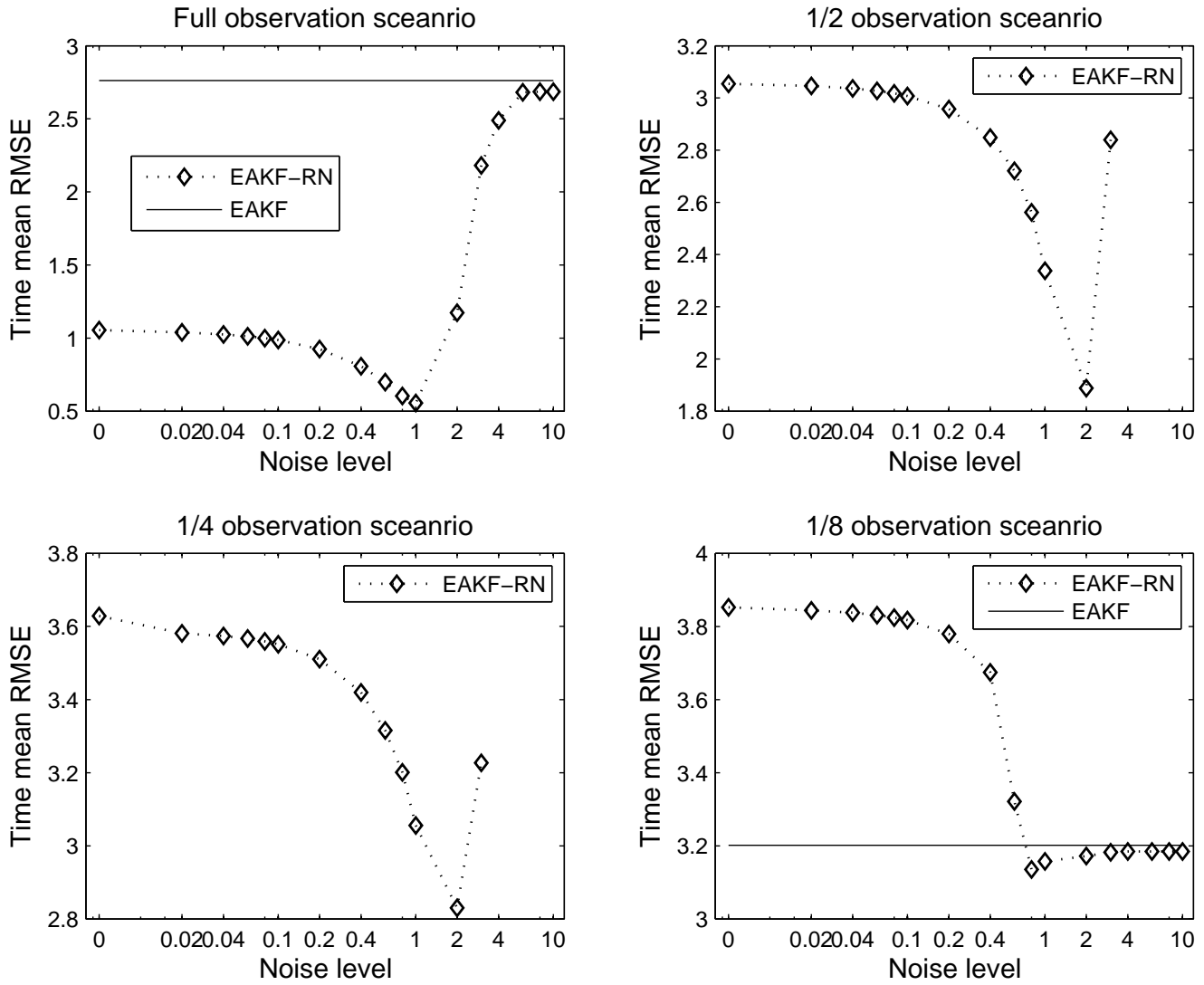


Figure 6. As in Fig. 5, but with $\lambda = 1.05$ and $l_c = 0.3$ for both the filters. Note that in the 1/2 and 1/4 observation scenarios divergences of the normal EAKF are spotted, hence no horizontal lines are indicated in the corresponding plots. The EAKF-RN also diverges in the 1/2 and 1/4 observation scenarios for $\beta \geq 4$.

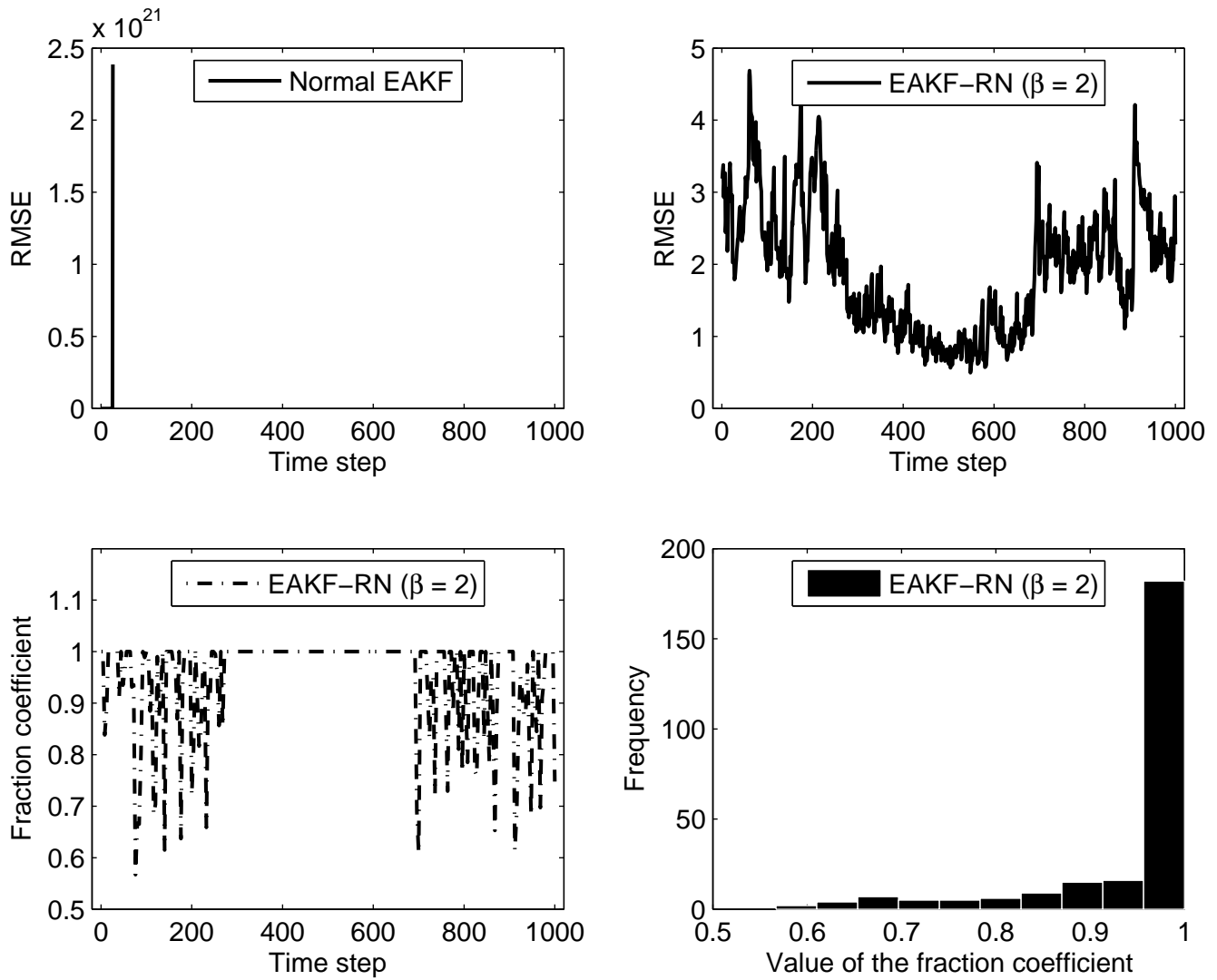


Figure 7. Upper left: sample time series of the RMSE of the normal EAKF in the 1/2 observation scenario; Upper right: sample time series of the RMSE of the EAKF-RN ($\beta = 2$) under the same experiment settings as the EAKF; Lower left: corresponding fraction coefficient c_k in the EAKF-RN ($\beta = 2$); Lower right: corresponding histogram of c_k .

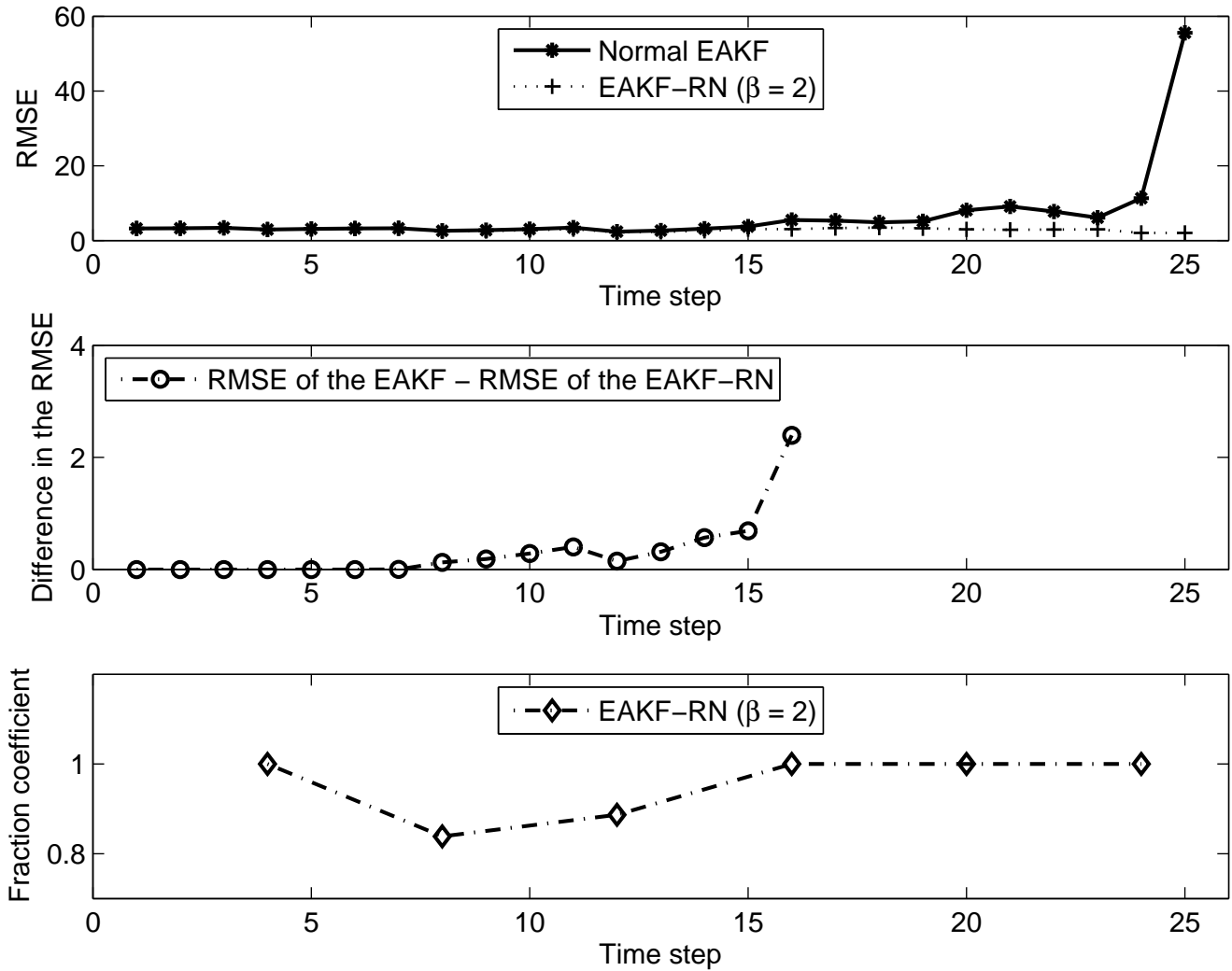


Figure 8. Upper: the RMSE of the EAKF (solid line with asterisks) and EAKF-RN ($\beta = 2$, dotted line with plus signs) between the time instant $k = 1$ and $k = 25$; Middle: difference in the RMSE ($=$ RMSE of the EAKF - RMSE of the EAKF-RN) between $k = 1$ and $k = 16$; Lower: the fraction coefficient of the EAKF-RN ($\beta = 2$) between $k = 1$ and $k = 25$.

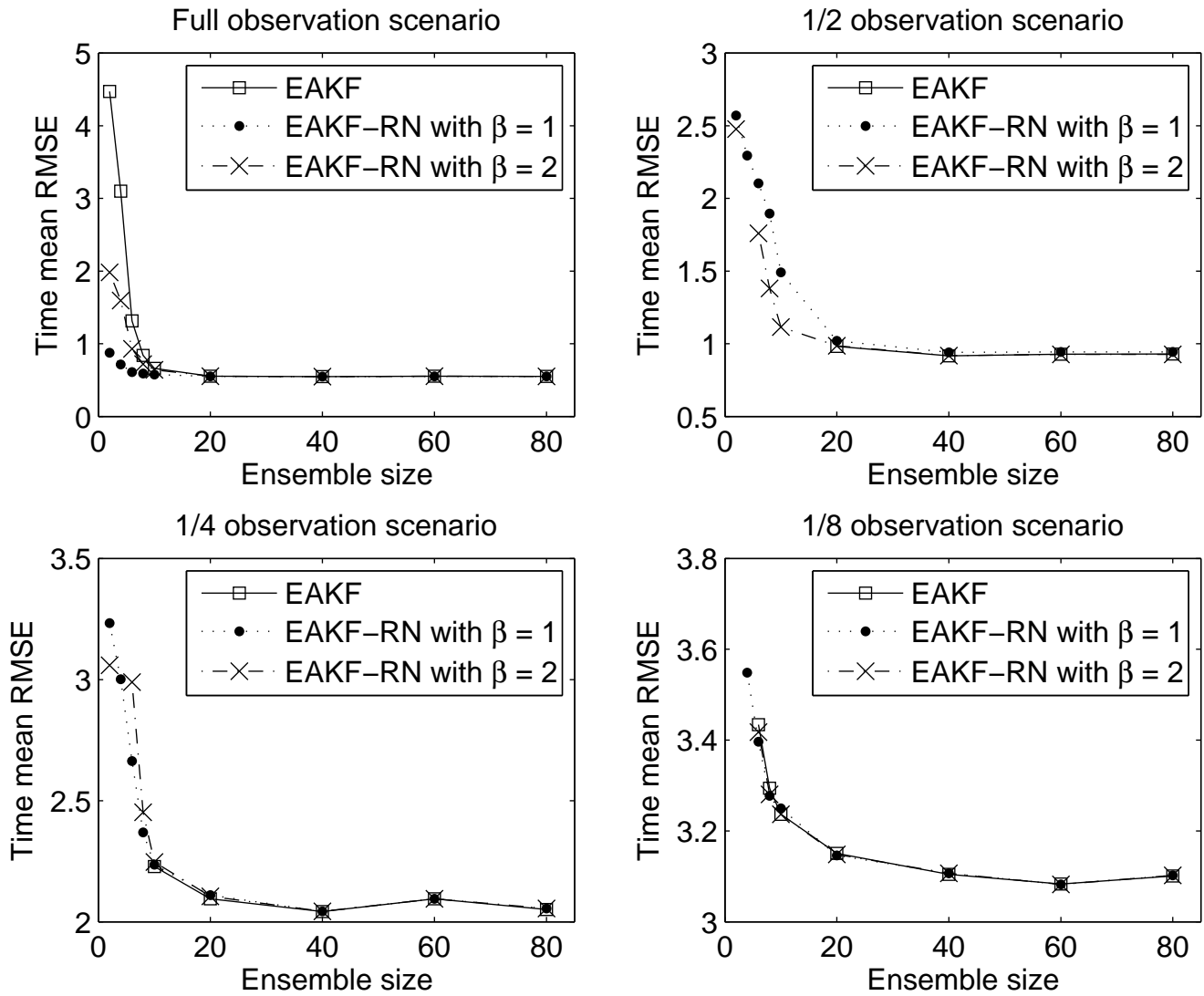


Figure 9. Time mean RMSEs of the EAKF and the EAKF-RN, as functions of the ensemble size in different observation scenarios.

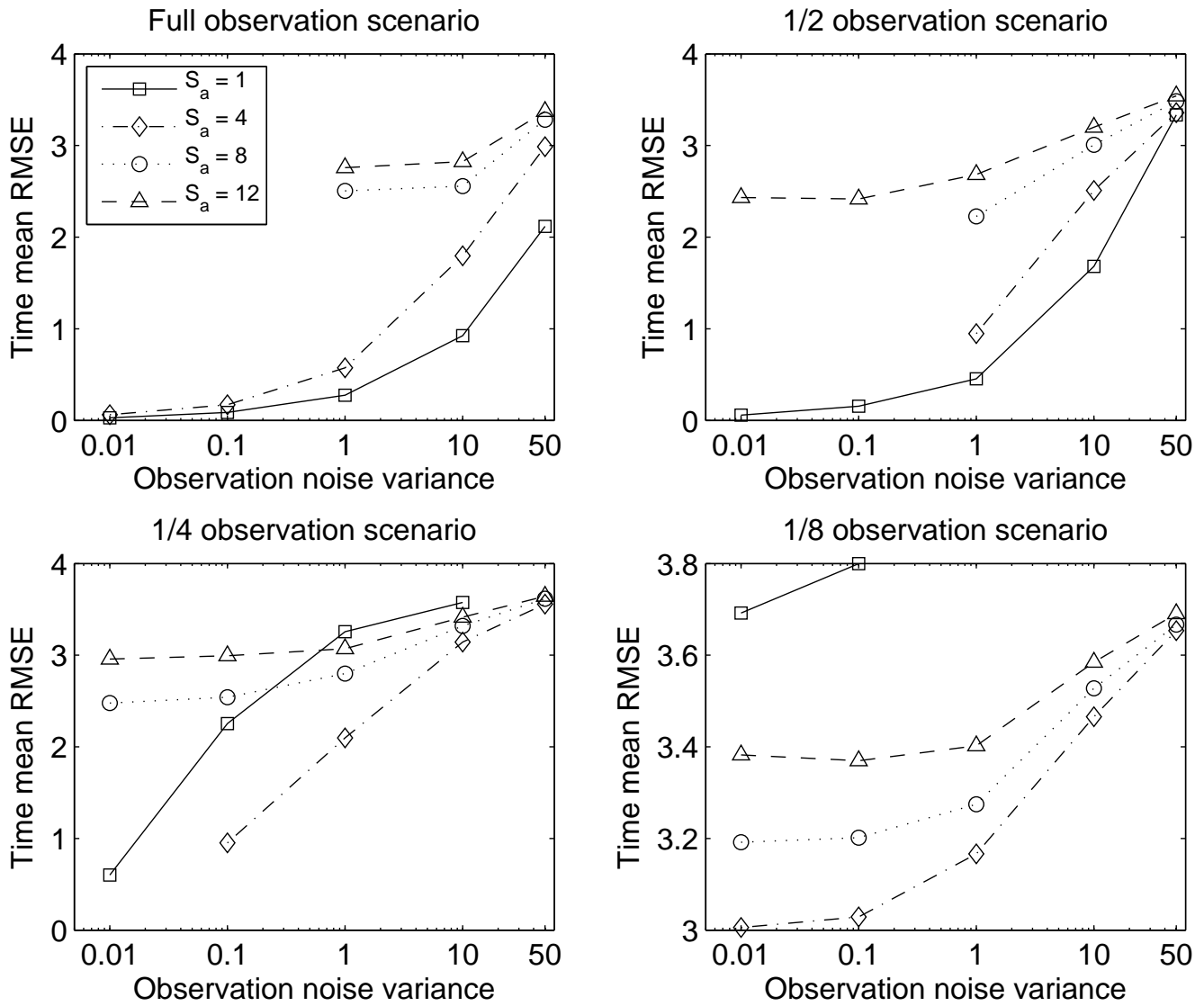


Figure 10. Time mean RMSEs of the normal EAKF, as functions of the assimilation step S_a and the observation noise variance, in different observation scenarios.

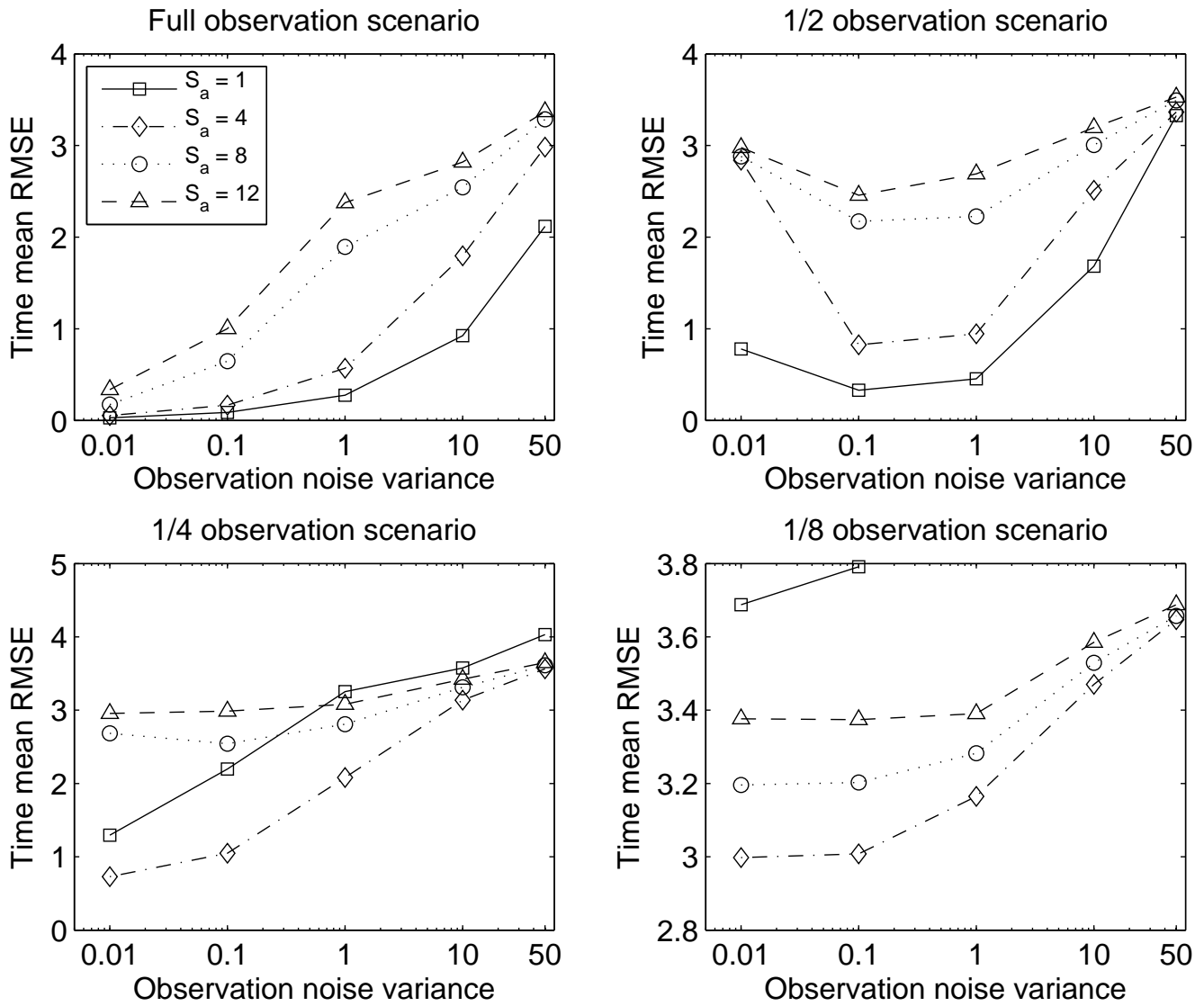


Figure 11. As in Fig. 10, but for the EAKF-RN with $\beta = 2$.

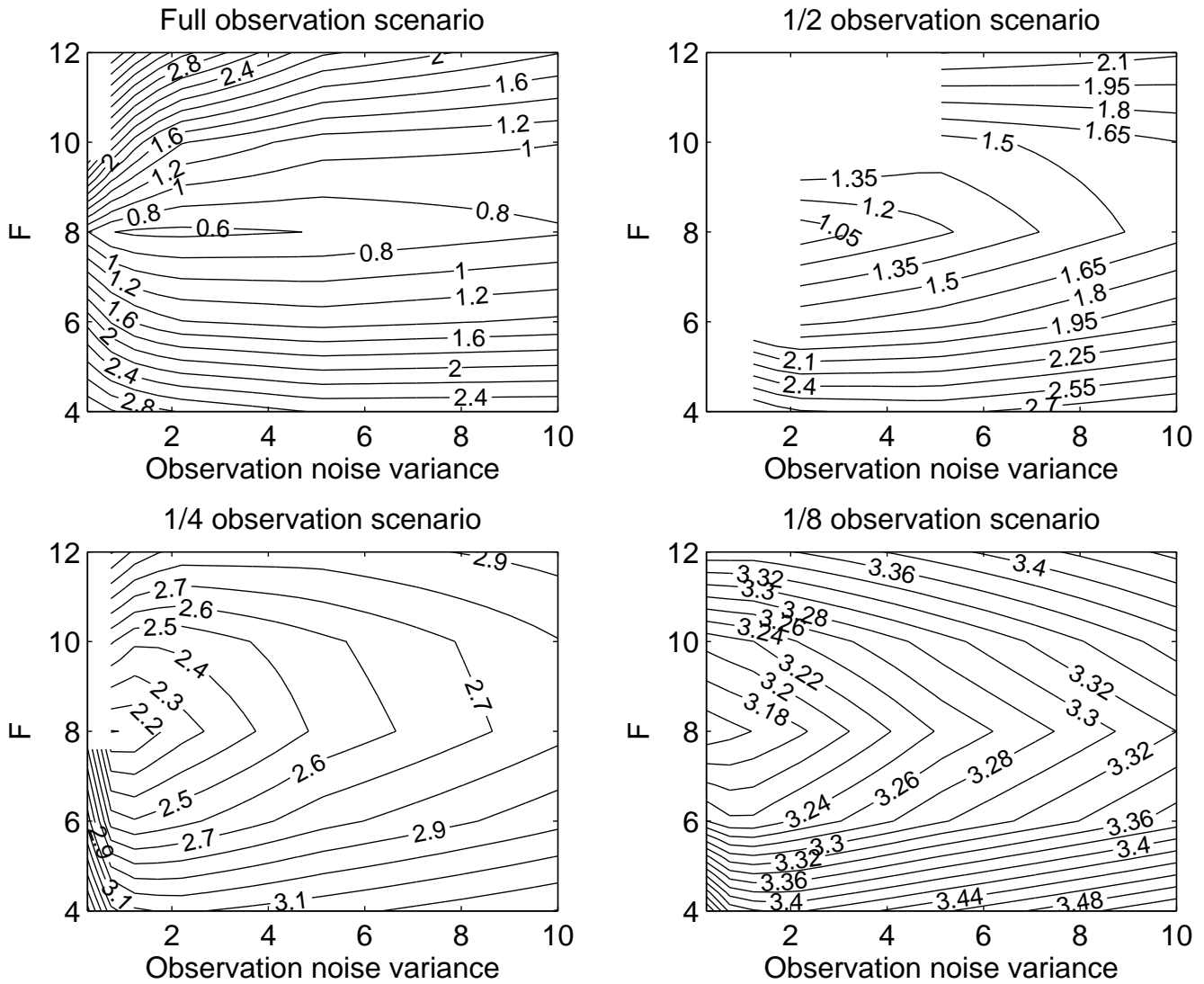


Figure 12. Time mean RMSEs of the EAKF, as functions of the (possibly) mis-specified driving force F and the observation noise variance γ , in different observation scenarios.

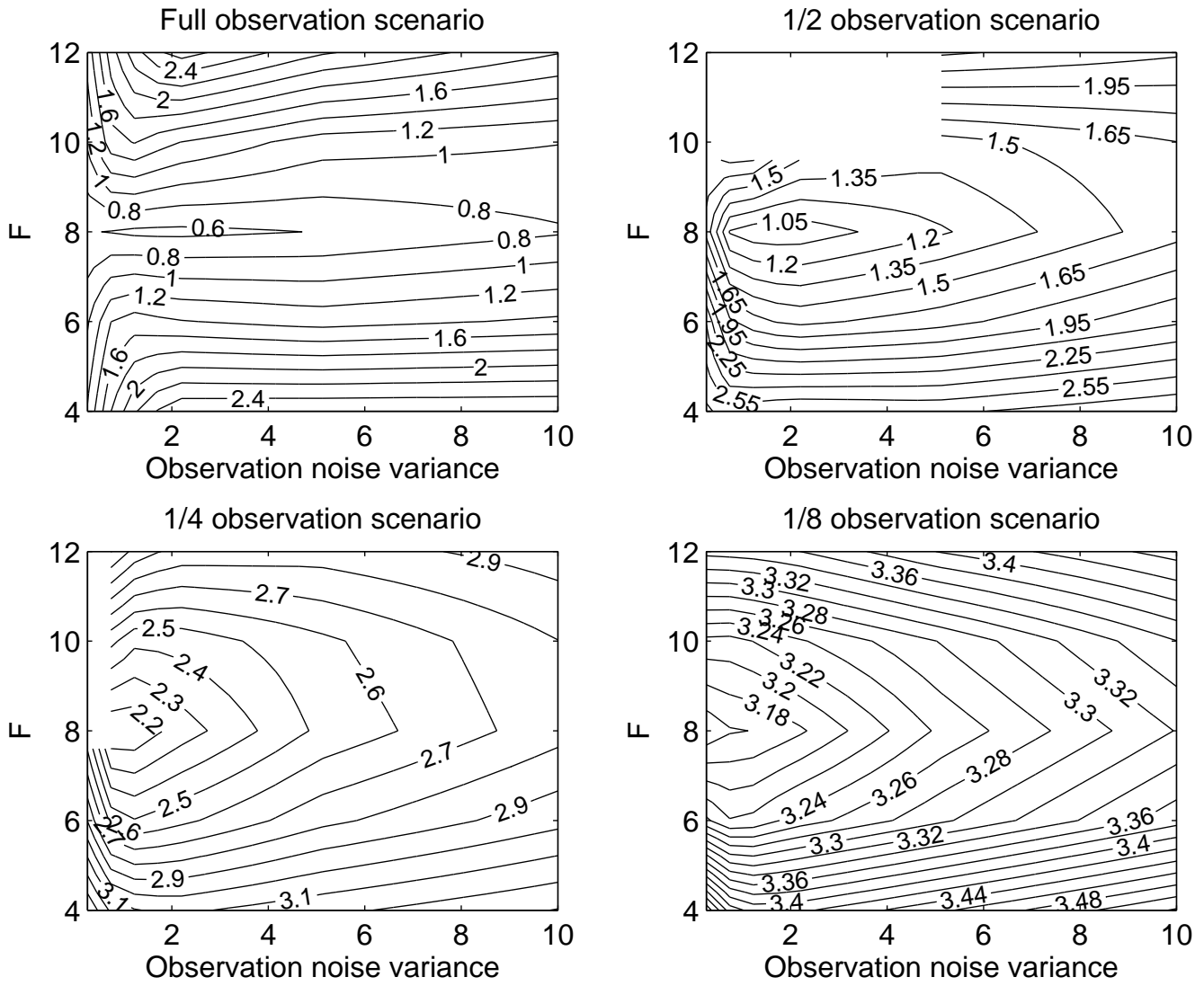


Figure 13. As in Fig. 12, but for the EAKF-RN with $\beta = 2$.